Surface segregation of Sn and Sb in the low index planes of Cu

by

Joseph Kwaku Ofori Asante

MSc.

This thesis is submitted in accordance with the requirements for the degree

Philosophiae Doctor

in the Faculty of Natural and Agricultural Sciences,

Department of Physics,

at the

University of the Free State

Bloemfontein

Republic of South Africa

Promoter : **Prof. W. D. Roos**

Co-Promoter: **Prof. J.J. Terblans**

May 2005

ACKNOWLEDGEMENTS

The author wishes to express his sincere appreciation to the following:

- *Almighty GOD,* for his expressed mandate to the author in Gen.1:28.
- *Prof. WD Roos*, the author's promoter, for his knowledge and great ideas in the field of this subject.
- *Prof. JJ Terblans,* the author's co-promoter, for his assistance in the running of the ternary computer programme and fruitful discussions
- *My wife, Sylvia*, children: *Kofi, Kobby, Akosua* and *Nhyira* for their great support.
- *Prof. HC Swart,* the Head of the Department of Physics (UFS), for his concerns and interest in this subject..
- The personnel of the Department of Physics (UFS), for their assistance and support.
- The personnel of the Division of Instrumentation (UFS), for their assistance.
- The personnel of the Division of Electronics (UFS), for their assistance.
- *Pastor At Boshoff*, CRC, my great spiritual head for his teachings from the Word of God.
- *Pastor Andre Lombard,* my zone pastor for his prayers.

Summary

In this study, the segregation parameters for Sn and Sb in Cu were determined for the first time using novel experimental procedures. Sn was first evaporated onto the three low index planes of Cu(111), Cu(110) and Cu(100) and subsequently annealed at 920 ^{o}C for 44 days to form three binary alloys of the same Sn concentration. Experimental quantitative work was done on each of the crystals by monitoring the surface segregation of Sn. Auger electron spectroscopy (AES) was used to monitor the changes in concentration build up on the surface by heating the sample linearly with time (positive linear temperature ramp, PLTR) from 450 to 900 K and immediately cooling it linearly with time (negative linear temperature ramp, NLTR) from 900 to 650 K at constant rates. The usage of NLTR, adopted for the first time in segregation measurements, extended the equilibrium segregation region enabling a unique set of segregation parameters to be obtained.

The experimental quantified data points were fitted using the modified Darken model. Two supportive models – the Fick integral and the Bragg-Williams equations - were used to extract the starting segregation parameters for the modified Darken model that describes surface segregation completely. The Fick integral was used to fit part of the kinetic section of the profile, yielding the pre-exponential factor and the activation energy. The Bragg-Williams equations were then used to fit the equilibrium profiles yielding the segregation and interaction energies. For the first time, a quantified value for interaction energy between Sn and Cu atoms through segregation measurements was determined (Ω_{CuSn} = 3.8 kJ/mol). The different Sn segregation behaviours in the three Cu orientations were explained by the different vacancy formation energies (that make up the activation energies) for the different orientations. The profile of Sn in Cu(110) lay at lowest temperature which implies that Sn activation energy was lowest in Cu(110).

Sb was evaporated onto the binary CuSn alloys and annealed for a further 44 days resulting in Cu(111)SnSb and Cu(100)SnSb ternary alloys. Sn and Sb segregation measurements were done via AES. The modified Darken model was used to simulate Sn

and Sb segregation profiles, yielding all the segregation parameters. Guttman equations were also used to simulate the equilibrium segregation region that was extended by the NLTR runs to yield the segregation and interaction energies. These segregation values obtained from the modified Darken model for ternary systems completely characterize the segregation behaviours of Sn and Sb in Cu. For the ternary systems, it was found that Sn was the first to segregate to the surface due to its higher diffusion coefficient, which comes about mainly from a smaller activation energy ($E_{Sn(100)}$ = 175 kJ/mol and $E_{Sb(100)}$ = 186 kJ/mol). A repulsive interaction was found between Sn and Sb (Ω_{SnSb} = - 5.3 kJ/mol) and as a result of the higher segregation energy of Sb, Sn was displaced from the surface by Sb. This sequential segregation was found in Cu(100) ($\Delta G_{Sb(100)}$ = 84 kJ/mol; $\Delta G_{Sn(100)}$ = 65 kJ/mol) and in Cu(111) ($\Delta G_{Sb(111)}$ = 86 kJ/mol; $\Delta G_{Sn(111)}$ = 68 kJ/mol). It was also found that the profile of Sn in the ternary systems lay at lower temperatures due the higher pre-exponential factor ($D_{oSn(binary)}$ = 9.2 × 10^{-4} m^2/mol and $D_{oSn(ternary)}$ = 3.4 × 10^{-3} m^2/mol) if compared to the binary systems.

This study successfully and completely describes the segregation behaviour of Sn and Sb in the low index planes of Cu.

Contents

CHAPTER ONE

INTRODUCTION

Today, both simple and sophisticated metallurgical products are found in all aspects of modern life, both domestic and industrial. There is still an ongoing search for better material properties for a great number of applications such as corrosion resistance, integrity of materials at high and low temperatures, wear resistance and weight reduction.

With the limited world natural resources but growing demand for material (metallurgical) products, it is becoming imperative for material and surface science researchers to properly understand the behaviour of each material within its multi-parameter environment so that its best use could be defined. Most material products come in the form of alloys. From a metallurgical point of view, alloying elements could either be undesirable impurities or deliberate dopants in the alloying system. It is also becoming imperative to seek possible alternatives for elements with a limited or uncertain source. The factors of high cost and time of production of material products must also be decreased.

As materials are developed, inevitable problems associated with their usage under various conditions are coming to the fore and these demand scientific understanding and solutions. A case in point is the well-known inter-granular fracture in the rotor of the Hinkley Point Power Station turbine generator [1,2]. During a routine test in 1969, one of the many 3Cr-0.5Mo steel rotors disintegrated and destroyed much of the turbine installation [3]. The other rotors were found to be safe, indicating that the disintegration of the odd one was not a characteristic of the steel type and its heat treatment. Upon much scientific scrutiny of the broken parts, made possible with many surfaces and grain boundary techniques like Auger Electron Spectroscopy (AES), it was discovered that the segregation of impurities (mainly P) in the steel to the grain boundary sites caused the temper brittleness in the alloy and hence the rotor's disintegration. A large number of research investigation have been done on ferrous systems where high- and low-temperature grain boundary fragility have been shown to be associated with the segregation of elements like As, Cu, Sn, Sb and S [4-7]. Knowledge of these impurities that caused embrittlement and their effects could be countered by the deliberate introduction of other elements (like rare earth metals such as La) that could also segregate to the grain boundaries to reject and neutralize these embrittling species [8]. Other problems associated with impurity segregation in alloys are inter-granular corrosion [9,10] and hydrogen embrittlement due to catalytic activity [11].

It is common practice in the field of microelectronics to coat Cu alloys contact with Sn, a process called "electrotinned" in order to minimise interface degradation [12]. It has also been found, however, that every tin-plated Cu alloy experiences the formation of copper-tin inter-metallic compounds (Cu_6Sn_5 and Cu_3Sn) at the interface of the tin and the base metal [13]. With time and/or increase in temperature, the inter-metallic compound moves

towards the surface and can adversely affect contact resistance and solderability. The inter-metallic growth could be retarded, however, by using a "barrier metal" (a metal that diffuses much, much more slowly with the base alloy and tin) [14]. Also, by allowing the segregation of Cu to the grain boundaries in Al thin film conductors electro-migration may be reduced considerably [15].

In the field of materials science and surface science, segregation of one or more components to interfaces and surfaces can influence both the physical and chemical properties of the alloy [16]. Some important areas that could be affected by grain boundary and surface segregation include crystal growth, catalysis, semi-conducting interfaces and the mechanical strength of solids. Indeed, for multi-component alloys, segregation can induce the formation of two-dimensional compounds at the surface [17-21]. These could be stabilised epitaxially and have different, better physical properties such as two-dimensional conductivity, superconductivity and magnetism compared to that of their individual constituents' [22]. Surface and interfacial segregation plays a major role in the heat treatment of alloys and are therefore of great technological importance [23].

Another field of study involving segregation is in nanoparticles. One recent study [24] involved Monte Carlo simulations of the segregation of Ni in Pt-Ni nanoparticles. Thin films of Pt-Ni inter-metallic alloy have been used as electro-catalysts in the lower temperature polymer electrolyte fuel cells [25]. However, besides the Pt-Ni nanoparticle having high surface-volume ratio, it has been found that $Pt_{75}Ni_{25}$ nanoparticle form a surface-sandwich structure with Pt atoms enriched in the outermost and third layers, while the Ni atoms are enriched in the second atomic layer as a result of surface segregation.

This nanoparticle elemental arrangement is very cost effective and places the Pt atoms at highly desirable position in its usage as electro-catalyst, as compared to that of a thin film.

The above narration therefore point to a very important phenomenon, called the segregation of impurities in alloys. The phenomenon has received the attention of surface scientists for over a century now [26].

1.1 The segregation phenomenon

Surface segregation is commonly regarded as the redistribution of solute atoms between the surface and the bulk of a material, resulting in a solute surface concentration that is generally higher than the solute bulk concentration. The redistribution comes about so that the total energy of the crystal is minimised [27]. For a closed system, where pressure and temperature are the same for an interface and adjacent bulk, Gibbs free energy can be equated to the total energy. The Gibbs free energy is the sum of chemical potentials of the various constituents in the system. Equilibrium conditions may then be expressed as a function of the chemical potential terms instead of the total energy. The change in chemical potential terms connects the energetic factors that are the segregation and the inter-atomic interaction energies. In terms of these energetic factors therefore, surface phenomenon can also be regarded as the energy cost of transferring one impurity atom from the interior of a host crystal to its surface [28,29]. Surface structure and composition depend strongly on surface segregation energy. Two distinct contributions responsible for surface segregation are the strain energy due to the atomic size mismatch between the solute and the solvent, as well as the differences in their surface energies

[30]. Thus the solute that has a different atomic size as well as lower surface energy than the solvent will therefore segregate and enrich the surface in the solid solution alloy so as to minimize the Gibbs free energy.

When metal alloys are heated, the solute atoms of lower surface energy as compared to the solvent may move from within thousands of layers deep inside the bulk toward the surface. The movement of solute atoms within the bulk-solvent-matrix also constitutes diffusion, which comprises the activation energy and the pre-exponential factor. The pre-exponential factor in tend, is made up of the vibrational frequency and entropy terms [31]. The activation energy is made up of vacancy formation energy of the solvent and the solute atom migration energy [32]. Segregation parameters are then regarded as some energetics and diffusion factors that contribute in bringing about the phenomenon of surface segregation. These are the segregation, activation and the interaction energies as well as the pre-exponential factor. By measuring these solute enrichments on the surface as a function of temperature or time, their segregation parameters can be determined [33].

While there have been substantial efforts in examining surfaces of pure elements and the studies of the surface behaviours of binary alloys are rapidly developing, there is a gap in experimental knowledge of more complex multi-component alloys [34]. Yet a better understanding of alloy surface properties and more so, the knowledge of segregation parameters of the constituents in an alloy would be highly desirable and could even lead to advances in the ability to effectively design alloys for surface related applications. The acquisition of segregation data on the various alloying elements, through surface and grain boundary segregation research works with further theoretical considerations and could lead to the manufacturing of super alloys.

1.2 The objective of this work

The main objective of this study was to establish an experimental procedure to determine segregation parameters in a binary and ternary all-metal-alloy systems.

The procedure followed was to:

1. Prepare binary alloys of Cu(100), Cu(110) and Cu(111) single crystals with the same Sn concentration.

2. Measure and compare the segregation behaviour of Sn in each of the three Cu crystals using the AES technique with the method of linear temperature ramp (LTR). Do simulations of the experimental data via the modified Darken model.

3. Extend the binary alloys to ternary by adding the same quantity of Sb concentration to Cu(100)Sn, Cu(111)Sn and Cu(110)Sn.

4. Measure and compare the segregation behaviour of alloying elements Sn and Sb in each of the ternary systems using AES with the method of positive (PLTR) as well as negative (NLTR).

5. Use the Guttman equilibrium segregation equations to fit the experimental data from the NLTR runs to yield the segregation energies of Sn and Sb as well as the interaction energies between the atoms of Sn, Sb and Cu.

6. Extract the segregation parameters of Sn and Sb in the three low index Cu planes by fitting the modified Darken ternary segregation theory to the experimental results.

7. Compare the solute Sn segregation behaviour in the binary to that of the ternary.

1.3 The outline

This thesis is divided into five chapters. In **chapter 2**, the segregation theory and models for the binary and ternary systems that were used to interpret experimental results are given. On the binary systems, the Fick integral and the Bragg-Williams equations will be given. The shortcomings of these theories will be highlighted. The Regular Solution Model that accounts for the interaction between the different atoms will be given in conjunction with the modified Darken model for the binary alloy system. In the case of the ternary systems, the Guttman Ternary Regular Solution (TRS) model, also known as the equilibrium segregation equations, will be highlighted. Finally, the modified Darken equations for the ternary alloy that explains the complete segregation profile will be given.

In **Chapter 3**, the experimental set-up is given. The sample preparation, apparatus and the experimental procedures are discussed. Also given in this chapter is how the segregation measurements were conducted. The surface enrichment measurements of a segregating species via AES are the Auger peak-to-peak heights (APPH). These must be quantified to surface concentration in molar fractional terms. The quantification approach

involving the low energy electron diffraction (LEED) patterns will be given in this chapter.

Experimental results follow in **Chapter 4**. These include all the experimental data points and their calculated theoretical fits in graphical form. Sn segregation in the binary systems: Cu(100)Sn, Cu(110)Sn and Cu(111)Sn will be treated first. Quantitative assessment of the behaviour of Sn in the binary crystals in the form of segregation parameters will be made. The behaviour of Sn and Sb in the ternary alloy systems will also be treated quantitatively.

Chapter 5 will be for discussions and conclusions. Segregation of Sn in the binary CuSn will be treated first. Comparison of the rate of segregation of Sn will be given in the three orientations. The progression study of Sn segregation from binary to ternary will be investigated. Sn and Sb segregation in the Cu(100) and Cu(111) will be compared. An attempt will be made to compare the segregation behaviour of Sn in the binary as well as the ternary alloy systems.

CHAPTER TWO

THEORY

2.1 Introduction

A total description of surface segregation embraces both the kinetic and the equilibrium processes [35]. Darken described the phenomenon as an uphill diffusion as far as the concentration gradient is concerned [36]. The measured intensity versus temperature or time from the AES technique gives a combined kinetic and equilibrium segregation profile of the surface. From the kinetic region the diffusion parameters, pre-exponential

factor D_o, and the activation energy E could be extracted [37]. The data making up the equilibrium segregation profile can also be used to get the other segregation parameters, namely, the interaction coefficient between the atoms i and j, Ω_{ij}, and segregation energy ΔG_i. At the onset of segregation, the segregation energy is responsible for driving the solute atoms from the first bulk layer to the surface. This creates a depleted layer and a concentration gradient between the depleted first layer and the rest of the bulk layers resulting in atomic flux toward the surface [38]. A number of models [39-42] are already in place to explain the segregation process. These models can be classified into two: one which essentially consists of special solutions of the macroscopic transport equations and the other with models describing the transport processes at a microscopic scale via jump probabilities of atoms of neighbouring atom layers [43].

The segregation models used in the present study are based on the macroscopic transport equations. These are the Fick, Bragg–Williams, Guttman and the Darken models. This study involves segregation in binary as well as ternary systems. In the following sections, the theories governing the binary systems will be treated first and will be followed by that on ternary systems.

2.2 Fick theory for binary alloys

One of the solutions to Fick's second law of diffusion,

$$\frac{\partial X}{\partial t} = D\frac{\partial^2 X}{\partial x^2} \tag{2.1}$$

where X is the concentration at the depth x after a time t and D is the coefficient of diffusion under the boundary condition: $X^{\phi} = 0$, at $x = 0$ for $t > 0$ and the initial condition: $X^{\phi} = X^{B}$, at $t = 0$ for $x > 0$ is:

$$X^{\phi} = X^{B}\left(1 + \frac{2}{d}\left(\frac{Dt}{\pi}\right)^{1/2}\right) \tag{2.2}$$

where X^{ϕ} is the solute surface concentration and d is the thickness of the segregated atom layer on the surface. **Equation 2.2** is appropriate for a binary alloy with segregating solute atoms of bulk concentration X^{B} and valid under the following conditions:

1) X^{ϕ} relates to short times t
2) For a constant diffusion coefficient
3) A homogenous concentration at $t = 0$.

Quite a number of researchers [44-50] have used **equation 2.2** to describe the time dependence of the segregated surface concentration at a constant temperature.

Du Plessis and Viljoen [51] first introduce the method of LTR whereby the temperature of the sample is ramped linearly with time, at a constant rate. They substituted t in **equation 2.2**, for temperature T according to:

$$t = \frac{T - T_o}{\alpha} \tag{2.3}$$

where T_o is the starting temperature, normally below a third of the melting point of the solute, so that sputtered-induced segregation can be neglected and α is the heating rate.

The diffusion coefficient D in **equation 2.2** can be replaced with the pre-exponential factor, D_o and the activation energy E according to the Arrhenius **equation 2.4**, below:

$$D = D_o \exp(-E/RT) \tag{2.4}$$

where R is the universal gas constant. Another concept, the enrichment factor, β, which is defined as

$$\beta = \frac{X^{\phi} - X^{B}}{X^{B}} \tag{2.5}$$

can be introduced into **equation 2.2**, to obtain the Fick integral equation:

$$\frac{1}{2}\beta^{2} = \frac{2D_o}{\pi \alpha d^2} \int_{T_o}^{T_E} e^{-E/RT} dT \tag{2.6}$$

where T_E is the temperature at the end of the kinetic region of the segregation profile. The solute surface concentration, X^{ϕ}, is then monitored by a surface sensitive technique such as Auger Electron Spectroscopy (AES) as a function of temperature or time. One important advantage of **equation 2.6** is that the increase in temperature is controlled and known at all stages as the solute segregates to the surface and it is thus possible to solve the diffusion equation for a given set of values of D_o and E. **Equation 2.6** accounts only for a certain range of temperatures in the kinetic part of the segregation profile and could only be used to fit experimental data in this range to extract the diffusion parameters D_o and E.

It is important, though, for the heating rate α to be very small so that more time is allowed for the atoms to move onto the surface [51-52].

After long times equilibrium segregation sets in and the Bragg-Williams equation can be used to describe this part of the process quite well.

2.3 The Bragg-Williams equation for binary alloys

The equilibrium conditions for a binary alloy, in terms of chemical potential terms μ_i^v is,

$$\mu_1^\phi - \mu_1^B - \mu_2^\phi + \mu_2^B = 0 \tag{2.7}$$

where i = 1, 2 represent the solute and the solvent atoms respectively and v, the phase: surface ϕ or the bulk B [35]. Each term in **equation 2.7** can be expanded via the regular solution model that takes into account the interactions between the atoms and was first developed by Hildebrand [53].

The regular solution model is based on three assumptions:

1) Atoms are randomly distributed over positions in a three-dimensional lattice
2) No vacancies exist
3) The energy of the system may be expressed as the sum of pair wise interactions between neighbouring atoms.

The model proposes that the interaction coefficients Ω_{ij}, in a regular solution, where the components have atomic concentrations X_i are related via the chemical potential energy and the activity coefficient f [54,55].

When **equation 2.7** is therefore expanded in terms of the regular solution model, the Bragg-Williams equilibrium segregation equation is obtained as:

$$\frac{X_1^{\phi}}{1-X_1^{\phi}} = \frac{X_1^{B}}{1-X_1^{B}} \exp\left[\frac{\Delta G + 2\Omega_{12}\left(X_1^{\phi} - X_1^{B}\right)}{RT}\right] \tag{2.8}$$

where $\Delta G = \mu_1^{oB} - \mu_1^{o\phi} - \mu_2^{oB} + \mu_2^{o\phi}$ is the segregation energy.

Equation 2.8 can be used to fit the data of the equilibrium section of the segregation profile to yield both the segregation energy ΔG and the interaction coefficient Ω_{12} [56].

Combining the Fick integral and the Bragg-Williams equations, however, do not completely describe the segregation process. The all-embracing model that describes both the kinetic as well as the equilibrium segregation process adequately, however, is the modified Darken model.

2.4 The modified Darken model

The modified Darken model considers the differences in the chemical potential energy between the multi-layers as the driving force behind segregation [57-59]. Atoms will move from the bulk, a region of high chemical potential, to the surface, a place of low chemical potential.

The original model [57] proposed that the net flux of species *i* (J_i) through a plane at x = *b* is given by:

$$J_i = -M_i X_i^B \left(\frac{\partial \mu_i}{\partial x} \right)_{x=b} \tag{2.9}$$

where M_i is the mobility of the species *i* and X_i^B the supply concentration in between two layers (within the plane). This supply concentration from within the planes has got no physical meaning and the first modification to the Darken model categorically associates the supply concentration to a specific layer as:

$$J_i^{(j+1,j)} = M_i X_i^{(j+1)} \frac{\Delta \mu_i^{(j+1,j)}}{d} \tag{2.10}$$

Equation 2.10 then indicates the flux of atoms from the (*j* + 1)-th layer to the *j*-th layer with the supply concentration $X_i^{(j+1)}$ and the difference in the chemical potential between

the layers $\mu_i^{(j+1,j)}$. The segregation system of surface ϕ and bulk *B* is therefore described by:

$$\frac{\partial X_i^{\phi}}{\partial t} = \left[\frac{M_i^{B_1 \to \phi} X_i^{B_1}}{d^2} \Delta\mu_i^{(B_1,\phi)} \right] \tag{2.11}$$

and for the *j*-th layer,

$$\frac{\partial X_i^{(j)}}{\partial t} = \left[\frac{M_i^{j+1 \to j} X_i^{(j+1)}}{d^2} \Delta\mu_i^{(j+1,j)} - \frac{M_i^{j \to j-1} X_i^{(j)}}{d^2} \Delta\mu_i^{(j,j-1)} \right] \tag{2.12}$$

for $i = 1,2, \ldots, m-1$ and $j = \phi, B_{1,\ldots N}$.

Now there are $(m-1)(N+1)$ rate equations for the $N+1$ layers.

2.4.1 The Darken rate equations for binary systems

For the binary alloy elemental composition $m = 2$, which implies that $i = 1$, is the solute in the alloy. The two rate equations for the surface and the first subsurface layers are:

$$\frac{\partial X_1^{\phi}}{\partial t} = \left[\frac{M_1^{B_1 \to \phi} X_1^{B_1}}{d^2} \Delta\mu_1^{(B_1,\phi)} \right] \tag{2.13}$$

$$\frac{\partial X_1^{B_1}}{\partial t} = \left[\frac{M_1^{B_2 \to B_1} X_1^{B_2}}{d^2} \Delta\mu_1^{(B_2,B_1)} - \frac{M_1^{B_1 \to \phi} X_1^{B_1}}{d^2} \Delta\mu_1^{(B_1,\phi)} \right] \tag{2.14}$$

where the mobility $M_1^B (= M_1^{B_2 \to B_1} = M_1^{B_1 \to \phi})$, which for a dilute alloy $= \frac{D_1}{RT}$ [60].

Equations 2.13, 2.14 and those of subsequent layers constitute a system of coupled non-linear differential equations and they make up the modified Darken model. Further, $\Delta\mu_1^{(B_1,\phi)}$ is expanded using the regular solution model and **equation 2.13** becomes:

$$\frac{\partial X_1^{\phi}}{\partial t} = \frac{M_1 X_1^{B_1}}{d^2}\left[\Delta G + RT\ln\frac{X_1^{B_1}\left(1-X_1^{\phi}\right)}{X_1^{\phi}\left(1-X_1^{B_1}\right)} + 2\Omega_{12}\left(X_1^{\phi} - X_1^{B_1}\right)\right] \tag{2.15}$$

and **equation 2.14** becomes:

$$\frac{\partial X_1^{B_1}}{\partial t} = \frac{M_1 X_1^{B_2}}{d^2}\left[RT\ln\frac{X_1^{B_2}\left(1-X_1^{B_1}\right)}{X_1^{B_1}\left(1-X_1^{B_2}\right)} + 2\Omega_{12}\left(X_1^{B_1} - X_1^{B_2}\right) - RT\ln\frac{X_1^{B_1}\left(1-X_1^{\phi}\right)}{X_1^{\phi}\left(1-X_1^{B_1}\right)} - 2\Omega_{12}\left(X_1^{\phi} - X_1^{B_1}\right)\right] \tag{2.16}$$

The system of $N + 1$ differential equations are integrated for a given set of parameters, $\Delta G_1, \Omega_{12}, M_1$ and X_1^B. In order to minimize boundary effects, N should be chosen as large as possible such as $N + 1 = 300$. The change in concentration rate of the 300-th layer is then considered zero. A rough estimate of the number of layers contributing to the flux of atoms to the surface is equal to the ratio of the maximum solute coverage to the bulk concentration times 100.

At equilibrium, the change in concentration rates of all the layers become equal to zero and the modified Darken rate equations convert to that of Bragg-Williams.

2.4.2 The Darken rate equations for ternary systems

In the case of a ternary alloy, m = 3, that is, there are two alloying elements besides the substrate and this yields two rate equations for each layer or cell of the crystal.

(a) The Rate Equations for the Surface Layer (ϕ) are given by:

For solute 1,

$$\frac{\partial X_1^{\phi}}{\partial t} = \left[\frac{M_1^{B_1 \to \phi} X_1^{B_1}}{d^2} \Delta\mu_1^{(B_1,\phi)} \right] \tag{2.13}$$

For solute 2,

$$\frac{\partial X_2^{\phi}}{\partial t} = \left[\frac{M_2^{B_1 \to \phi} X_2^{B_1}}{d^2} \Delta\mu_2^{(B_1,\phi)} \right] \tag{2.17}$$

According to the regular solution model, $\Delta\mu_i^{(B_1,\phi)}$ is a function of both the segregation energies ΔG_i and the interaction parameters Ω_{ij}, between the alloying elements or species as shown in **section 2.3.**

Selecting the equations of solute 1 for further analysis, from **equation 2.13**, the difference

in the chemical potential energy $\Delta\mu_1^{(B_1,\phi)}$ between the surface ϕ, and the first bulk layer B_1 is given by:

$$\Delta\mu_1^{(B_1,\phi)} = \mu_1^{B_1} - \mu_1^{\phi} + \mu_3^{\phi} - \mu_3^{B_1} \tag{2.18}$$

Each of these chemical potential energy terms is further expanded according to the regular solution model to give the final analytical expression.

At equilibrium, the rate of change in concentration in the layers equals zero and the equilibrium conditions become:

$$\mu_i^{\phi} - \mu_i^{B} - \mu_m^{\phi} + \mu_m^{B} = 0 \tag{2.19}$$

For the ternary system, however, i = 1, 2 and m = 3 and the equilibrium equations, in terms of chemical potential terms are:

$$\mu_1^{\phi} - \mu_1^{B} - \mu_3^{\phi} + \mu_3^{B} = 0 \tag{2.20}$$

$$\mu_2^{\phi} - \mu_2^{B} - \mu_3^{\phi} + \mu_3^{B} = 0 \tag{2.21}$$

Guttman [61] applied the regular solution model to the surface segregation in ternary alloys by way of expanding **equations 2.20** and **2.21** in terms of surface concentrations.

2.5 Guttman ternary equilibrium segregation equations

The expansion of each chemical potential term in **equations 2.20** and **2.21** via the activity coefficient and the interaction coefficient yields

$$X_1^{\phi} = \frac{X_1^B \exp(\Delta G_1 / RT)}{1 - X_1^B + X_1^B \exp(\Delta G_1 / RT) - X_2^B + X_2^B \exp(\Delta G_2 / RT)} \tag{2.22}$$

$$X_2^{\phi} = \frac{X_2^B \exp(\Delta G_2 / RT)}{1 - X_1^B + X_1^B \exp(\Delta G_1 / RT) - X_2^B + X_2^B \exp(\Delta G_2 / RT)} \tag{2.23}$$

where

$$\Delta G_1 = \Delta G_1^o + 2\Omega_{13}(X_1^B - X_1^{\phi}) + \Omega'(X_2^{\phi} - X_2^B) \tag{2.24}$$

$$\Delta G_2 = \Delta G_2^o + 2\Omega_{23}(X_2^B - X_2^{\phi}) + \Omega'(X_1^{\phi} - X_1^B) \tag{2.25}$$

Equations 2.24 and **2.25** indicate that element *i* will segregate to the surface if $\Delta G_i > 0$. Further, according to **equations 2.24** and **2.25**, there are three driving forces in the segregation energy ΔG_i. The first is the difference in standard chemical potentials between the surface and the bulk (ΔG_1^o); the second is the term in Ω_{i3} which could be called the self-interaction term and lastly, the term Ω', which takes into account the interactions between the solute atoms. The segregation energy ΔG_i will thus be positive for $\Omega_{i3} < 0$ and $\Omega' > 0$.

Equations 2.22, **2.23**, **2.24** and **2.25** indicate that equilibrium conditions are independent of the diffusion coefficients. The equations can be used to get the segregation energies ΔG_i and the interaction coefficients Ω_{ij} mathematically by fitting to the equilibrium values of the measured data. (See **annexure A** for the flow chart).

2.6 Summary

The short time *t* constraint that is related to the temperature interval T_E and T_o place on the Fick integral also shows its disadvantage. The Fick integral can however be used to give the starting parameters to the Darken model if appropriate temperature intervals in the kinetic region could be selected. The values extracted from the Bragg-Williams equations also serve as starting values for the modified Darken model in the case of the binary alloy of Cu and Sn.

For the Cu, Sn and Sb ternary alloy, Guttman equilibrium segregation equations are also used to fit the segregation data (the high temperature region of the PLTR experimental values and also the data points for the NLTR) mathematically to yield the segregation energies of the solutes as well as the interaction coefficients of all the alloying elements. The advantage here is that the numbers of fit segregation parameters that are to be determined manually, in the solution of the modified Darken rate equations for the ternary alloy, are reduced to only diffusion coefficients and activation energies (but even here, the values obtained for Sn from the binary system could be used as starting values).

CHAPTER THREE

EXPERIMENTAL SETUP

3.1 Introduction

Sample preparation is a very important aspect of this segregation study. In this section, an account of the sample preparation and the experimental procedures that were followed will be given. The two surface techniques, Auger electron spectroscopy (AES) and low energy electron diffraction (LEED) will be described. This will be followed by AES quantification using LEED.

3.2 Sample Preparation

The Cu single crystals, all of 99.999% purity and cut along the (100), (110) and (111) planes and less than 1 degree orientation accuracy were ordered from Mateck, in Germany [62]. They were of the same diameter, 0.97 cm, and same thickness of 1.11 mm and polished below a roughness of 1 micron. Polycrystalline Cu rod of 99.99% purity and standards of Sb (purity 99.995%) were also ordered from Mateck. Sn (purity 99.995%) pellets, were obtained from Goodfellow Cambridge Limited [63]. Six dummy Cu polycrystalline samples were cut to similar sizes as the three crystals and mechanically polished up to 1 μ m using a diamond suspended solution.

All three Cu single crystals together with the six dummy polycrystalline Cu samples were mounted side-by-side on a carousel and introduced into an evaporation chamber, **figures 3.1** and **3.2**. A 50 k $\mathring{A}$ thick layer of Sn was deposited simultaneously onto the back face of the three Cu single crystals and the six dummy polycrystalline Cu samples

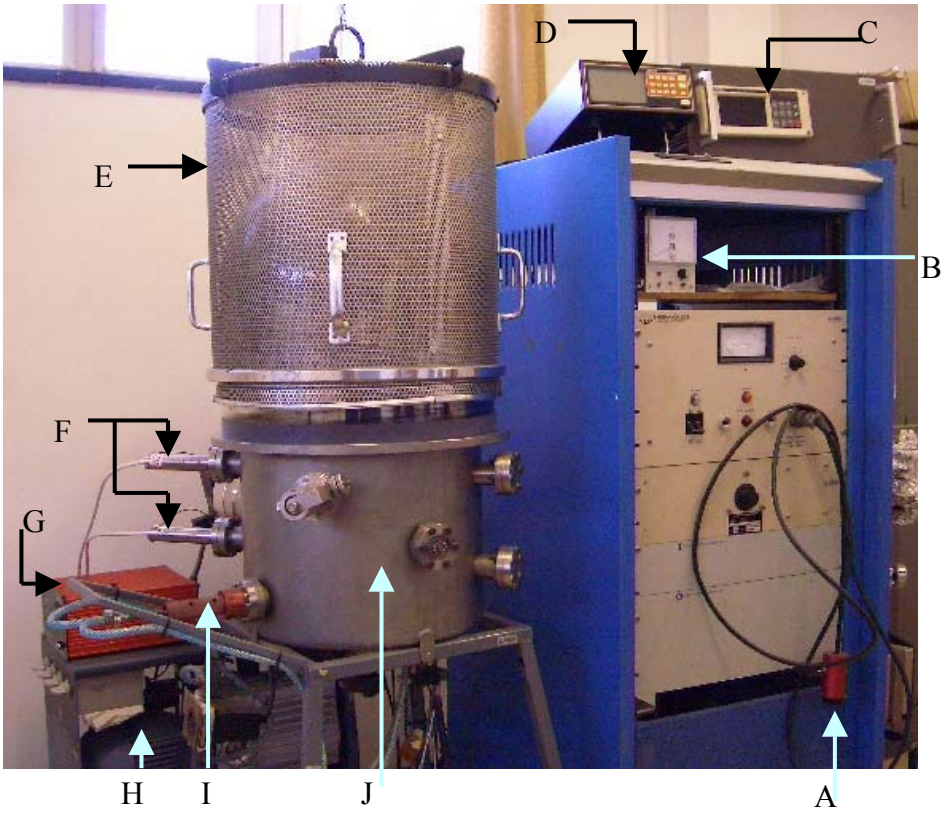

Figure 3.1 The evaporation system showing some of the external parts. **A**: electron gun filament current controller; **B**: Pirani gauge unit; **C**: Varian pressure gauge control unit; **D**: Inficon unit that indicates the evaporation rate and the evaporant thickness; **E**: glass dome cover; **F**: high voltage feed throughs connecting the electron gun filament; **G**: turbo-pump control unit; **H**: rotary pump; **I**: crucible manipulator; and **J**: stainless steel casing. Other parts not in the picture include the turbo-pump and the ionisation pressure gauge.

The block diagram of the inside components of the evaporation chamber is also shown in **figure 3.2**.

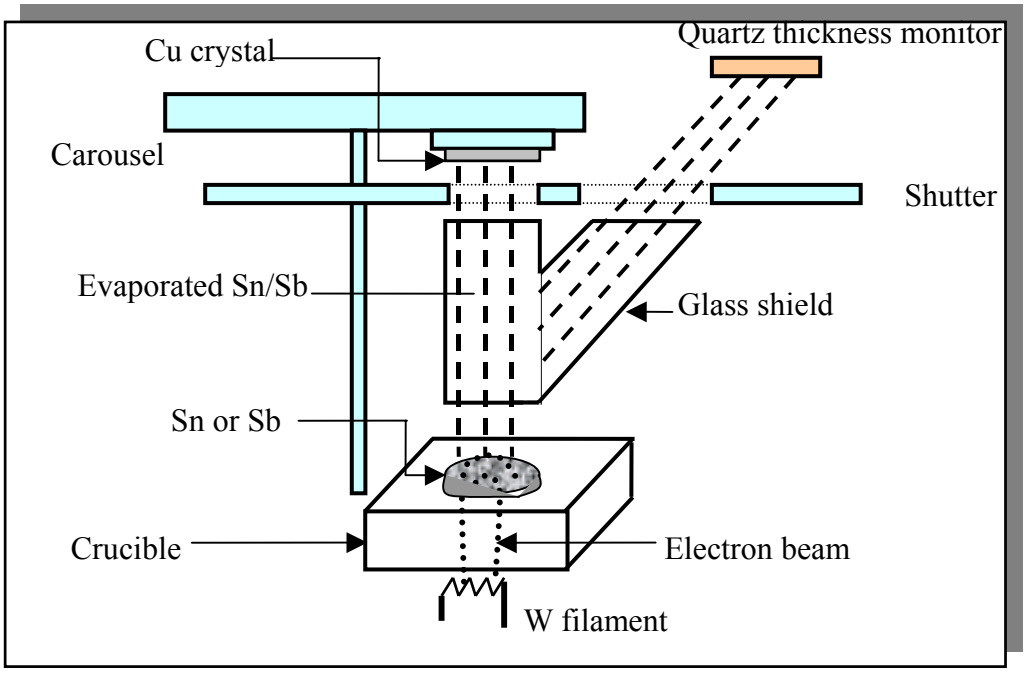

Figure 3.2 The evaporation system where Sn and Sb were evaporated onto the three Cu crystals and the six poly-crystals.

Further detailed photograph of the crucible is given in **figure 3.3**.

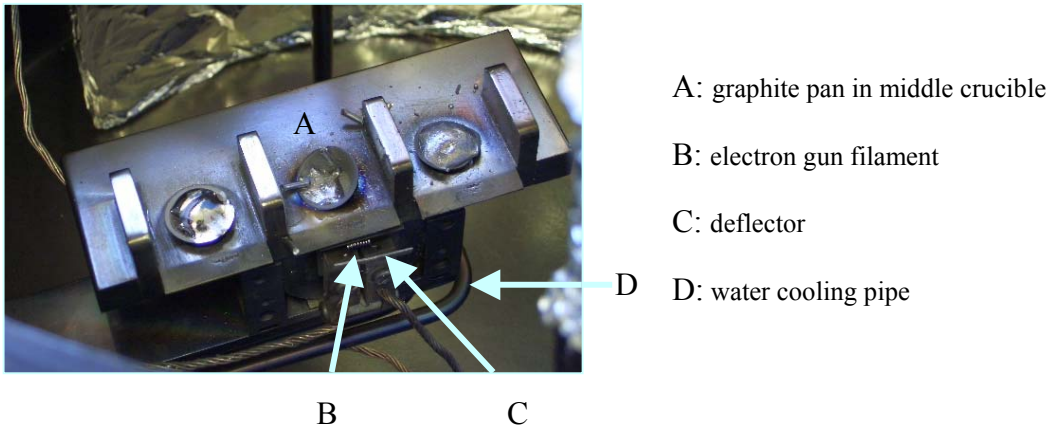

Figure 3.3 The three crucible compartments in the evaporation system. The central crucible is aligned with the electron gun filament **B**. The stream of electrons emitted are magnetically deflected and focused onto the substance to be evaporated in the graphite pan **A**.

The crystals with the adhered evaporant were put in quartz tubes that had two protruding openings as in **figure 3.4**. A steady but a slow flowing Ar gas source was connected to opening A. When the entire tube was filled with Ar after a duration of 2 minutes, opening B was heated till it became soft and was clamped and sealed. With the Ar gas still flowing but at a reduced rate, tube A was also quickly sealed. The whole quartz tube was then immersed in a beaker of acetone to check for any leakage.

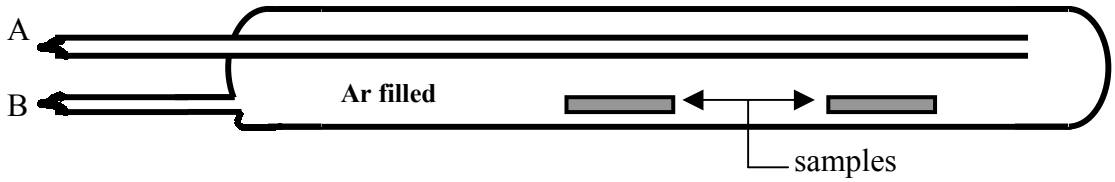

Figure 3.4 The sealed (openings A and B) quartz tube filled with Ar gas with the sample ready for annealing at 920 ^{o}C.

The tube was then transferred to the oven (see **figure 3.5**) and annealed at 920 ^{o}C for 44 days for above 99 % homogeneous mixture (according to dissolution equation in Crank [64]) of Sn atoms in the Cu matrix.

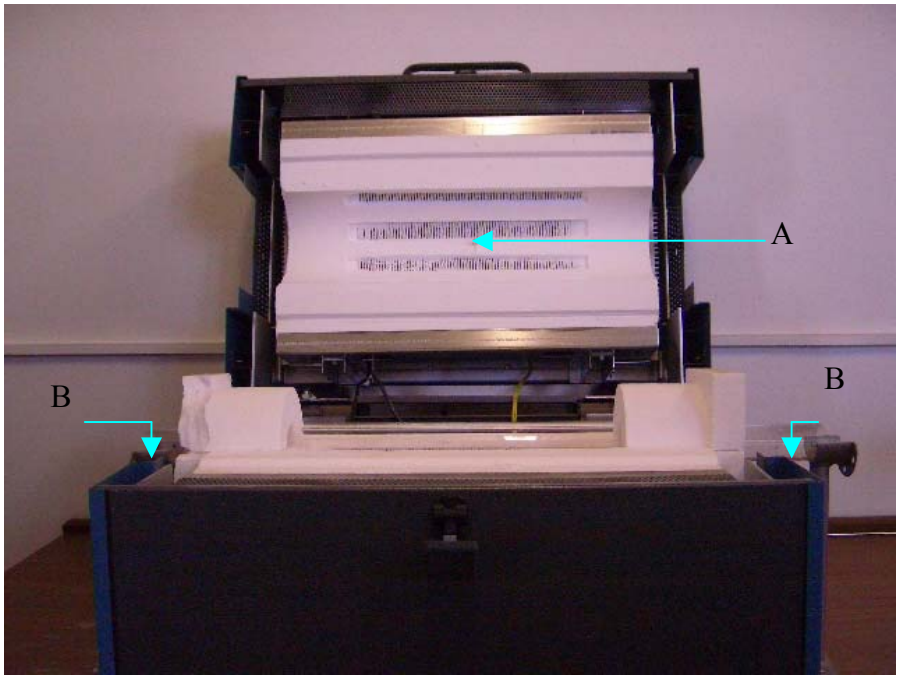

Figure 3.5 The annealing unit showing the thermo-couple junction **A** and the open-ended quartz tube **B** into which is inserted the smaller sealed quartz tube with the crystals, as in **figure 3.4**.

After annealing, atomic adsorption spectroscopy (AAS) measurements were done on two of the dummy samples and the bulk concentration of Sn found to be 0.145 ± 0.012 at. %.

Both AES and LEED measurements were then taken on each of the three CuSn single crystals under the same experimental conditions.

The next step was to evaporate 40 k Å Sb layer onto Cu(100)-Sn, Cu(110)-Sn and Cu(111)-Sn binary alloys as well as three other dummy samples simultaneously. The crystals were again sealed in quartz tubes under Ar gas atmosphere and annealed at 920 °C for 44 days for a homogeneous mixture of Sn and Sb atoms in the Cu matrix. Unfortunately, the Cu(110)SnSb crystal was oxidised during the annealing process and

had to be discarded. AAS measurements were done on two of the dummy samples and the bulk concentration of Sb found to be 0.121 ± 0.015 at. %.

AES measurements were also carried out on the two ternary Cu(100)SnSb and Cu(111)SnSb crystals under the same experimental settings.

3.3 Sample mounting and cleaning

Each of the single Cu alloys was mounted side-by-side with the standard samples of Cu, Sb and Sn onto a carousel of the AES system as shown in **figures 3.6** and **3.7**.

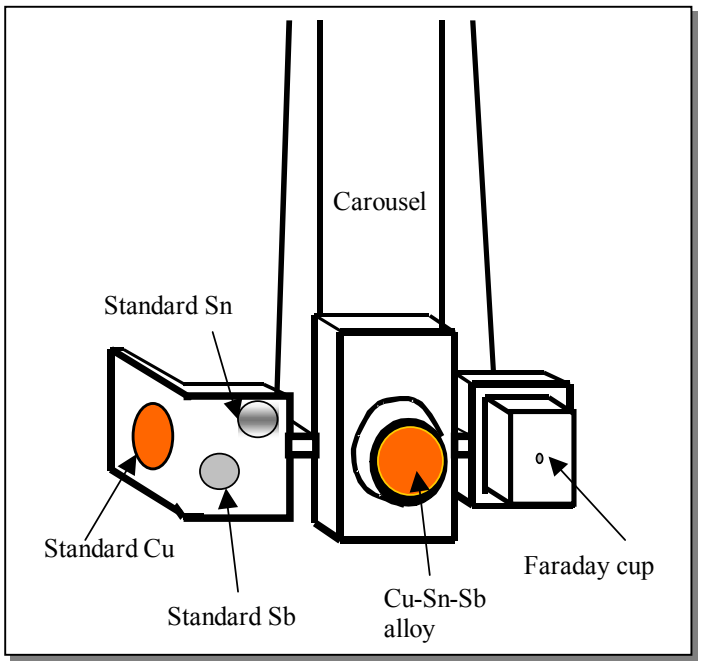

Figure 3.6 The arrangement of the crystals onto the carousel in the AES system

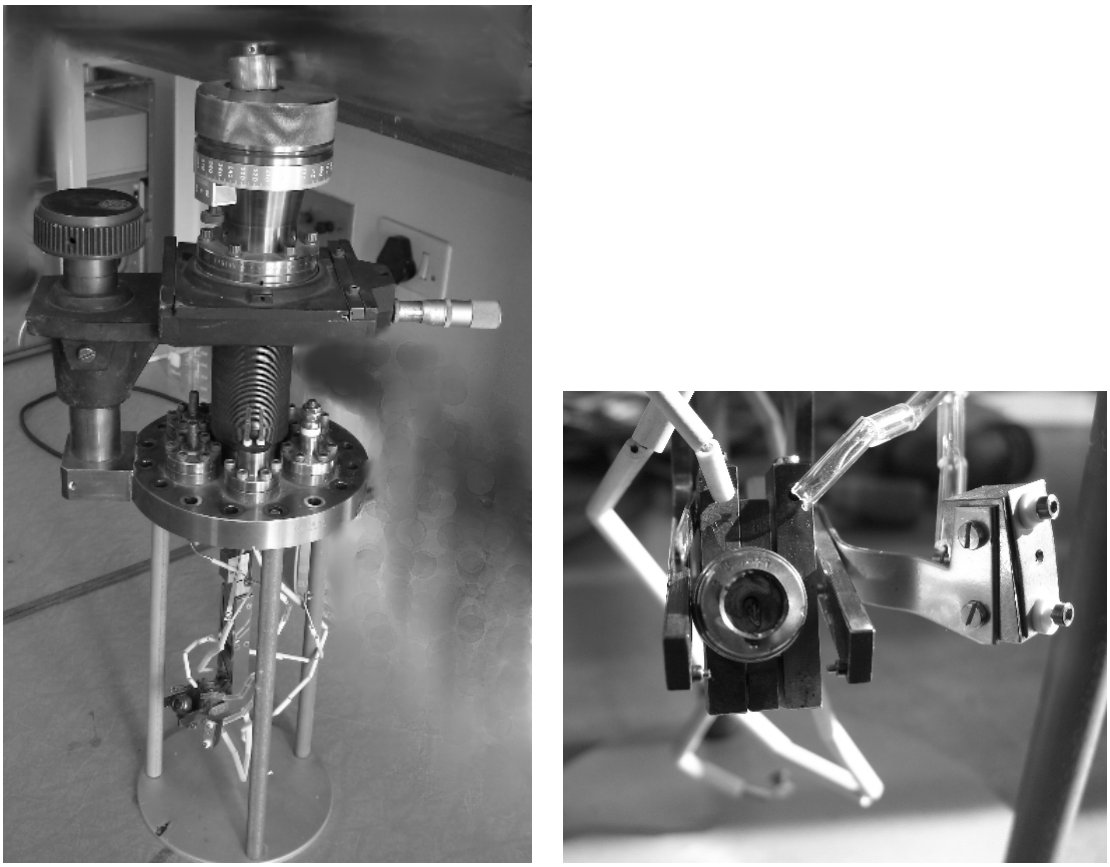

(a) (b)

Figure 3.7 (a) The flange housing the carousel on a stand and the sample manipulators and **(b)** a detailed photograph of the sample holder with a Faraday cup to its right. Notice also, the insulating wiring for the heater element as well as that for the thermocouple.

A detailed sketch of how each of the single Cu alloys was mounted onto a resistance heater is given in **figure 3.8**.

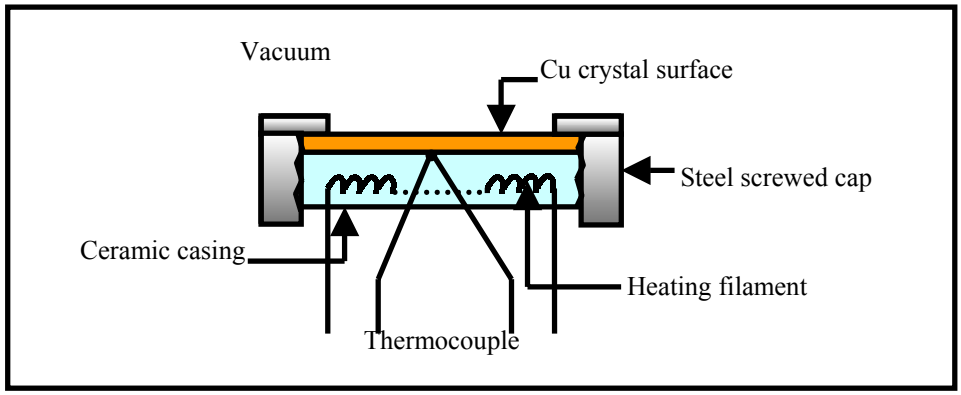

Figure 3.8 Section of the sample holder housing and the components for temperature measurements.

The junction of the chromel-alumel thermocouple was embedded in a ceramic slab (see **figure 3.8**) upon which the back face of the crystal was mounted for the temperature measurements. The heating filament was also put in the same ceramic slab.

Before the AES and LEED measurements, the sample was first cleaned of surface contaminants (C, S, O) by using the following procedure:

1. The sample was sputtered at room temperature for few minutes using Ar^+ ions of energy 2 keV and ion current of 70 nA and rastered over an area of 3 mm × 3 mm.
2. It was then heated to a higher temperature (550 ^oC) to de-absorbed trapped O and sputtered again for 5 minutes
3. It was further heated to 650 ^oC for 10 minutes without sputtering so as to level off any concentration gradient [65].
4. The sample was then cooled down to 550^oC and sputtered for 5 minutes.
5. The cycle (steps 2 and 3) was repeated six times before a cleaned surface was obtained.

3.4 The AES/LEED system

The spectrometers consist of the following components as shown in **Figure 3.9.**

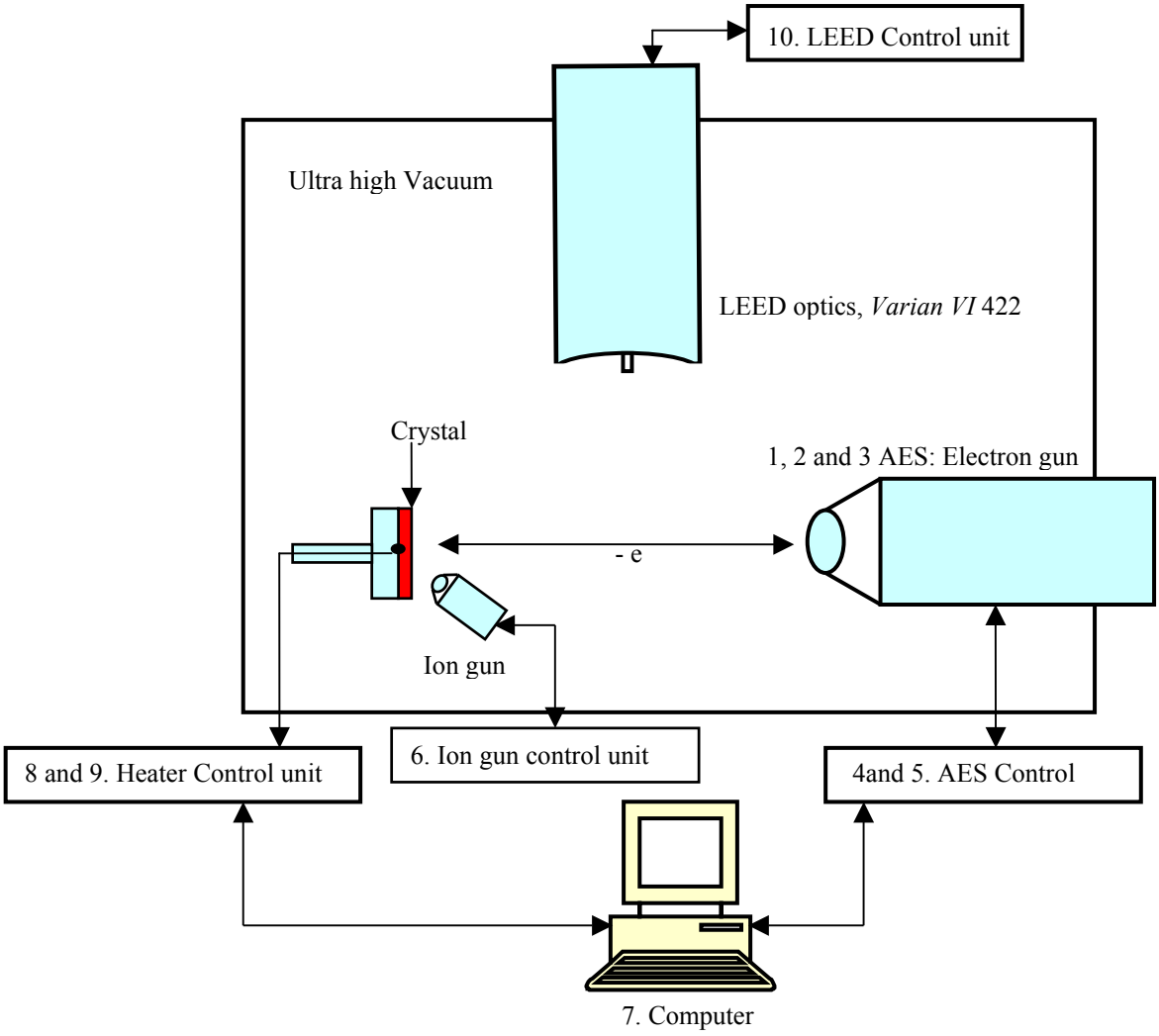

Figure 3.9 A block diagram describing the AES / LEED system

1. PHI 18-085 electron gun and control unit for providing the primary electron beam in the AES. In this study, the primary electron beam energy and current were 4 keV and 10 μ A respectively.

2. PHI 15-110B single pass cylindrical mirror analyzer (CMA) for electron energy analysis. It was used to measure the peak-to-peak height changes of Sn($M_5N_{45}N_{45}$), Sb($M_5N_{45}N_{45}$) and Cu($L_3M_{45}M_{45}$) peaks.
3. PHI 20-075 electron multiplier (high voltage supply) for providing high voltage to the electron multiplier inside the CMA. The voltage was 1150 V during measurements.
4. PHI 20-805 analyser control for the Auger signal set to modulation amplitude of 1 eV.
5. PHI 32-010 Lock-in-amplifier differentiating the Auger signal with a sensitivity of 10 mV and a time constant of 0.3 s.
6. The Perkin Elmer 11-065 Ion gun control and the Perkin Elmer 04-303 differential Ion gun for cleaning the sample's surface. The ion beam current was approximately 70 nA as measured with a Faraday cup, and accelerating voltage of 2 keV at a pressure of 5.2×10^{-5} torr.
7. A Computer was used for controlling and data acquisitions in the case of the AES.
8. A programmable temperature control unit capable of heating and cooling the sample at a set rate.
9. A chromel-alumel thermocouple unit was used to measure the varying temperature of the sample.
10. The LEED system was a *Varian Model VI 422*. LEED photos were taken of each of the samples before and after a LTR run. The LEED optics had a Varian 981-2145 electron gun unit and a Varian 981-2148 control unit.

3.5 The AES measurements

The AES was used to measure the peak-to-peak height changes of Sn($M_5N_{45}N_{45}$), Sb($M_5N_{45}N_{45}$) and Cu($L_3M_{45}M_{45}$) peaks in the derivative mode as a function of temperature. Measurements on each crystal was done under the following instrumental settings: base pressure 4.6×10^{-9} Torr, primary electron beam of energy 4 keV and current 10 μA, modulation energy 1 eV and a scan rate of 0.5 eV/s.

So far, most of the studies of interface segregation of dilute systems have been restricted to a treatment of segregation under isothermal conditions [66-68]. The constant temperature measurements demand at least three experimental runs at different temperatures and the use of an Arrhenuis equation in order to determine the diffusion parameters. It is not trivial to obtain exactly identical initial conditions for all measurements at the different temperatures. Normally, because of time constraints, constant temperature runs are done at temperatures where diffusion is already active and significant concentration of solute that had not been monitored already on the surface.

The above-mentioned problems were avoided by using the method of Linear Temperature Ramp (LTR) in the present segregation studies. Only one run is sufficient to get all the segregation parameters. Furthermore, the LTR run starts at low temperatures that correspond to low diffusion. For the first time, the LTR run was made to follow with two ramping routines: the constant heating of the sample, called the positive LTR (PLTR) and then constant cooling of the sample, the negative LTR (NLTR). In the PLTR runs, the computer was programmed to increase the crystal temperature from 150^{o}C at a specified

heating rate up to 630^{o}C. The NLTR runs followed immediately till the sample cooled to 450^{o}C. The heating and cooling rates considered were: ± 0.05^{o}C/s; ± 0.075^{o}C/s and ± 0.15^{o}C/s respectively and are appropriate for dilute substitutional alloy systems [69]. At the onset of a run, the sample was sputter cleaned for 3 minutes at 150 ^{o}C and AES spectrum of the cleaned surface was taken. The Sn (and Sb) surface concentration build-up as well as that of Cu were then monitored as a function of temperature for both PLTR and NLTR runs. Segregation runs for the different heating and cooling rates were done on each of the crystals. By cooling the sample slowly and linearly with time, the equilibrium segregation profile region was extended resulting in the attainment of more accurate set of equilibrium segregation parameters [70].

AES spectra were taken at the end of each run, making sure that there were no other segregating elements except Sn (and Sb, for the ternary). After a combined PLTR and NLTR runs, the crystal was heated again and remained at that temperature for more than 6 hours to annul any concentration gradient before the next run.

3.6 AES quantification from LEED patterns

The measured Auger peak-to-peak height (APPH) in the derivative mode can be quantified to surface concentration in atomic percentage in two ways. There is the approach that relates the APPH in the derivative mode of an element A, I_A, to the atom density (in atoms/m^3) of the element ($N_A(z)$), at a depth z from the surface, apart from other parameters as [71]:

$$I_A = I_o \sigma_A(E_o)[\sec\alpha] R_m(E_A) T(E_A) D(E_A) \int_0^\infty N_A(z) \times \exp\left[-\frac{z}{\lambda_m(E_A)\cos\theta}\right] dz \qquad (3.1)$$

where I_o is the primary electron current, $\sigma_A(E_o)$ is the ionization cross section of atom A for electrons with energy E_o, α is the angle of incidence of the primary electrons, $R_m(E_A) = 1 + r_m(E_A)$ and $r_m(E_A)$ is the back scattering term dependent on both the matrix m and the binding energy for the core level electron involved in the transition, leading to an Auger electron with energy E_A, $T(E_A)$ is the transmission efficiency of the spectrometer, $D(E_A)$ is the efficiency of the electron detector, $\lambda_m(E_A)$ is the inelastic mean free path in the matrix m and $\theta = 42^o$, is the angle of emission.

This approach demands AES spectra of the pure standards of all the alloying elements at the same experimental conditions, in order to find the correct sensitivity factor to correlate the molar fraction X_A, to the AES signal intensity I_A.

The other approach is based on low energy electron diffraction (LEED) patterns and quite a number of researchers [72-74] have used this for AES quantification. LEED photos of the cleaned sample were taken at room temperatures before a run and showed only the atomic patterns of the substrate. After a run, the sample surface structure would be different as a result of segregation of the solute atoms from the bulk, and LEED photographs were taken again. One then could classify the over-layer structure in terms of the substrate structure by the so-called Wood's notation.

3.6.1 Cu(100)

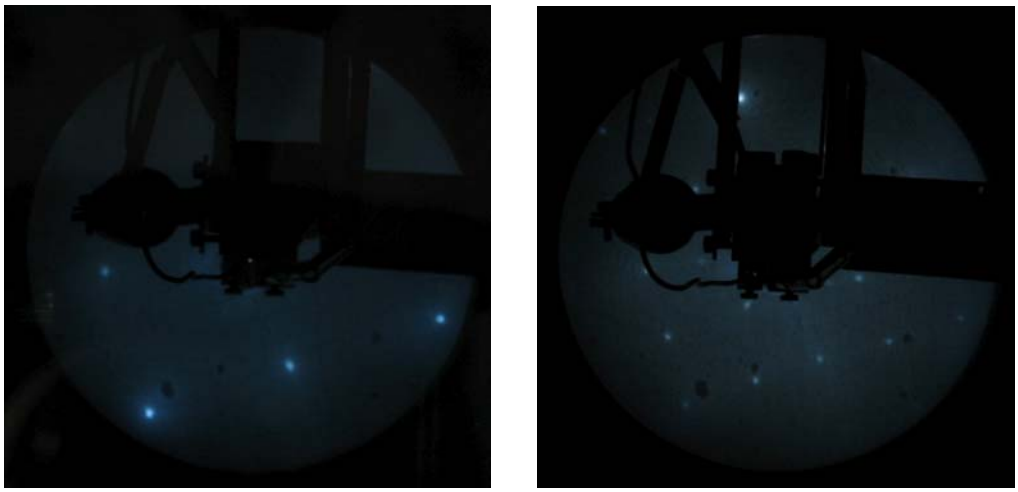

(a) **(b)**

Figure 3.10. LEED patterns of cleaned Cu(100) substrate (a) and with Sn segregate (b) at the same electron beam energy of 117 eV. The additional spots show another surface structure attributed to the presence of Sn atoms.

The observed LEED patterns however are (scaled) representations of the reciprocal net of the pseudo 2-D surface structures as shown in **figure 3.11** below.

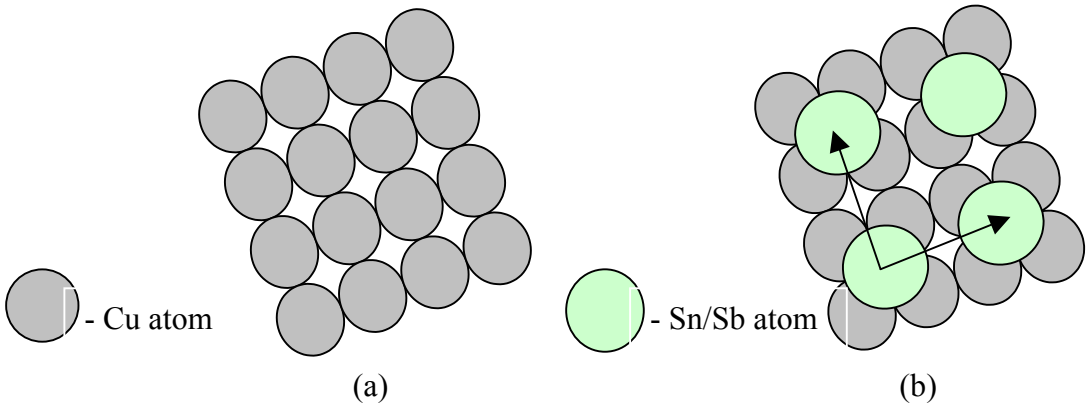

Figure 3.11. The real space of **(a)** cleaned Cu(100) crystal surface structure and the same surface but different structure after Sn segregation **(b)**.

From **figure 3.11**, it is clear that Sn forms a (2×2) overlayer structure on Cu(100) surface. If one considers the unit cell of the overlayer of Sn, the ratio of the segregated atoms to that of the Cu substrate is 1 : 4. The maximum Sn coverage is therefore 25 %.

The surface concentration of Sn is then calculated from:

$$X_{Sn}^{\phi}(T) = \frac{R_{Sn}(T)}{R_{eqm}^{\max}} \times 0.25 \tag{3.2}$$

where $R_{Sn}(T) = \frac{I_{Sn}(T)}{I_{Cu}(T)}$ the normalisation of which accounts for the possible shift in the peaks as a result of sample and holder expansion. $R_{eqm}^{\max}$ is the maximum value of $R_{Sn}(T)$ in the equilibrium region.

3.6.2 Cu(111)

(a) **(b)**

Figure 3.12. LEED patterns of cleaned Cu(111) substrate **(a)** and with segregated Sn **(b)** at the same electron beam energy of 117 eV. The additional spots show another surface structure attributed to the presence of Sn atoms.

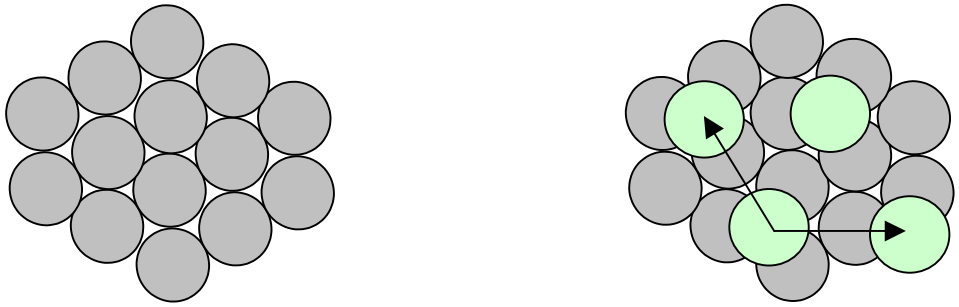

(a) **(b)**

Figure 3.13. The real space of **(a)** cleaned Cu(111) surface and the same surface after **(b)** Sn segregation.

From **figure 3.13 (b),** Sn forms a $(\sqrt{3}\times\sqrt{3})R30^{o}$ overlayer structure on Cu(111) surface. The unit cell of the overlayer Sn indicates the ratio of the number of the segregated atoms to Cu atoms as 1:3. The maximum Sn coverage is therefore 33.3 %.

The surface concentration of Sn was then calculated from:

$$X_{Sn}^{\phi}(T) = \frac{R_{Sn}(T)}{R_{eqm}^{\max}} \times 0.33 \qquad (3.3)$$

3.6.3 Cu(110)

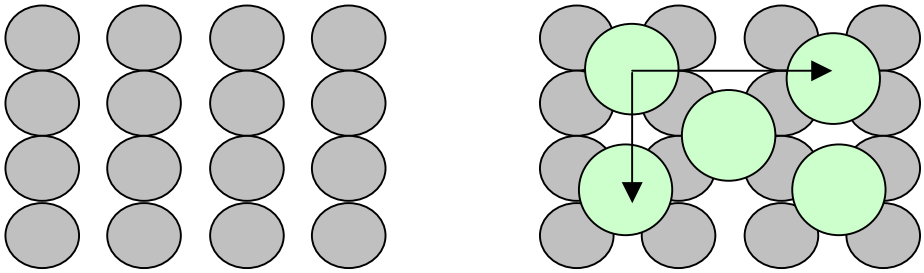

Figure 3.14. The real space of **(a)** cleaned Cu(110) surface and the same surface after **(b) Sn** segregation

From **figure 3.14**, Sn forms a c(2×2) overlayer structure on Cu(110) surface. The unit cell of the overlayer Sn, gives the ratio of the number of the segregted atoms to Cu atoms as 1: 2. The maximum Sn coverage is therefore 50 %.

The surface concentration of Sn is then calculated from:

$$X_{Sn}^{\phi}(T) = \frac{R_{Sn}(T)}{R_{eqm}^{\max}} \times 0.50 \qquad (3.4)$$

Similar equations to **3.2**, **3.3** and **3.4** hold for the surface concentrations of the alloying elements of Sn and Sb in the case of the ternary alloy, except that $R_{eqm}^{\max}$ in these cases is the maximum value of the sum of $R_{Sn}(T)$ and $R_{Sb}(T)$ at equilibrium.

CHAPTER FOUR

RESULTS

4.1 Introduction

In this chapter, four major results of which two have been published already [70,75] will be highlighted. The first deals with the consequences of the segregation behaviour of Sn in each of the three low index planes of Cu. It involves the binary system of Cu-Sn and the interaction energy between the atoms of Cu and Sn. The experimentally measured values will be given against the theoretical fittings that will embrace the Fick integral, the Bragg-Williams and the modified Darken equations. Sn segregation parameters in the three Cu single crystals will then be determined and compared.

The second part will involve the surface concentration measurements of Sn and Sb in Cu(100) ternary systems. The quantified experimentally measured values will be fitted with Guttman and the modified Darken equations and the segregation parameters of Sn and Sb will be extracted. The behaviour of the two alloying elements will be treated and compared.

The segregation behaviours of Sn and Sb in the two ternary alloys of Cu(100)SnSb and Cu(111)SnSb will be compared and the necessary deductions given.

Finally, the last part will see the progression study of Sn from binary Cu(111)Sn to ternary Cu(111)SnSb. As a result of atomic interactions, the segregation profile of Sn in the binary CuSn will be affected when another impurity, in this case Sb, is introduced to the binary CuSn. The extracted segregation parameters will be used to justify and explain the change in the segregation profile of Sn.

4.2 The binary Cu-Sn system

As was mentioned in **Chapter Two**, the Fick integral and the Bragg-Williams equations were used to fit some regions of the Sn segregation profile in the three Cu orientations. The extracted segregation parameters became the starting values for the main theory, the modified Darken equations that fit the complete segregation profile.

The calculated values of activation energies (E) of Cu in Cu in the three low index Cu planes are: $E_{(110)}$ = 162.3 kJ/mol, $E_{(100)}$ = 182.8 kJ/mol and $E_{(111)}$ = 204.5 kJ/mol [76].

These activation energies were considered to be the minimum values (the basis) in the search for both E and D_o in the three orientations.

Sn segregation results in Cu(100) is considered first followed by that of Cu(110) and lastly, Cu(111).

4.2.1 Cu(100)Sn binary system

4.2.1.1 The Fick integral fit

Figure 4.1 shows a measured PLTR run data comprising the kinetic segregation and equilibrium segregation profiles. Part of the kinetic segregation profile below the dotted temperature line A at 765 K, shows the region where the Fick integral was used to fit the measured data points to yield E and D_o as starting parameters for the modified Darken model.

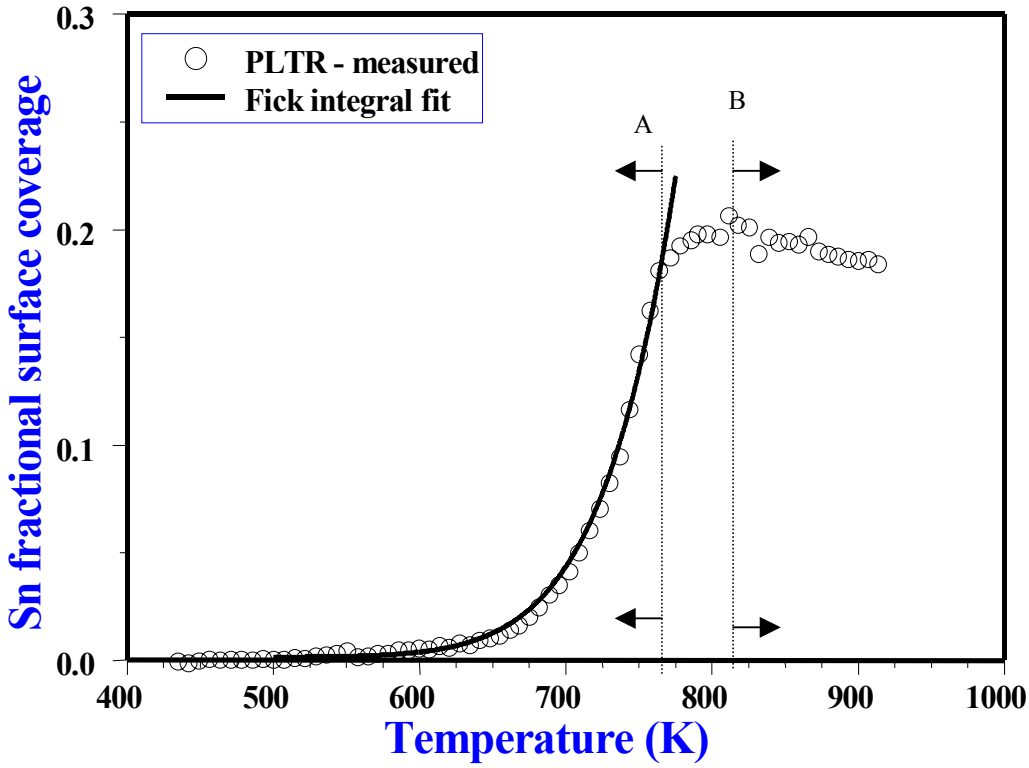

Figure 4.1 Measured Sn segregation in Cu(100) for PLTR run at heating rate of 0.05 K/s and the calculated Fick integral equation with $D_o = 6.2 \times 10^{-6}$ m^2/s and $E = 189$ kJ/mol.

Temperatures above the dotted temperature line B at 815 K indicate the equilibrium segregation part of the profile, which is a very narrow region that could be extended by cooling the sample linearly with time as shown in **figure 4.2**.

4.2.1.2 The Bragg-Williams fit

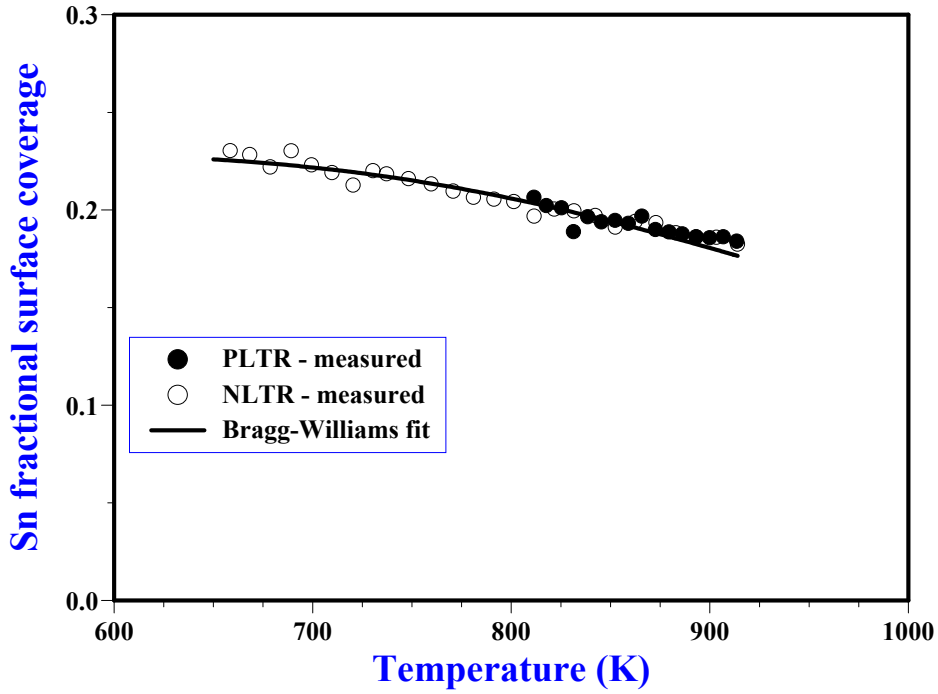

Figure 4.2 Measured Sn segregation in Cu(100) showing the equilibrium segregation profiles. Note the narrow region from the PLTR run and the extended part from the NLTR run. The calculated solid line is the Bragg–Williams fit for ΔG = 65 kJ/mol and Ω_{CuSn} = 4.1 kJ/mol. Sample's heating and cooling rates were ± 0.05 K/s respectively.

The segregation parameters E, D_o, ΔG and the Ω_{CuSn} obtained from the Fick integral and the Bragg-Williams equations were used as starting values for the modified Darken model. **Figures 4.3**, **4.4** and **4.5** show measured PLTR runs at different rates and their corresponding modified Darken fits.

4.2.1.3 The modified Darken fits

a) Sample heating rate: 0.05 K/s

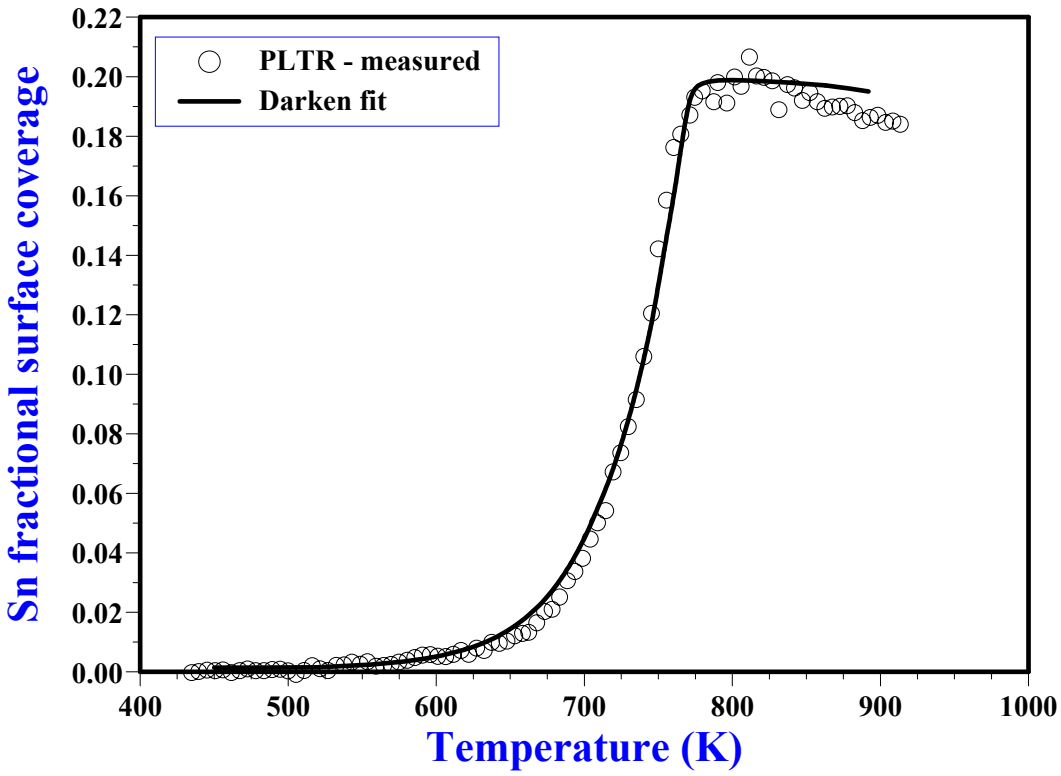

Figure 4.3 Measured Sn segregation in Cu(100) for PLTR run at heating rate of 0.05 K/s and the Darken model fit for segregation parameters: D_o = 6.2 × 10^{-6} m^2/s, E = 189 kJ/mol, ΔG = 65 kJ/mol and Ω_{CuSn} = 3.9 kJ/mol.

b) Sample heating rate: 0.075 K/s

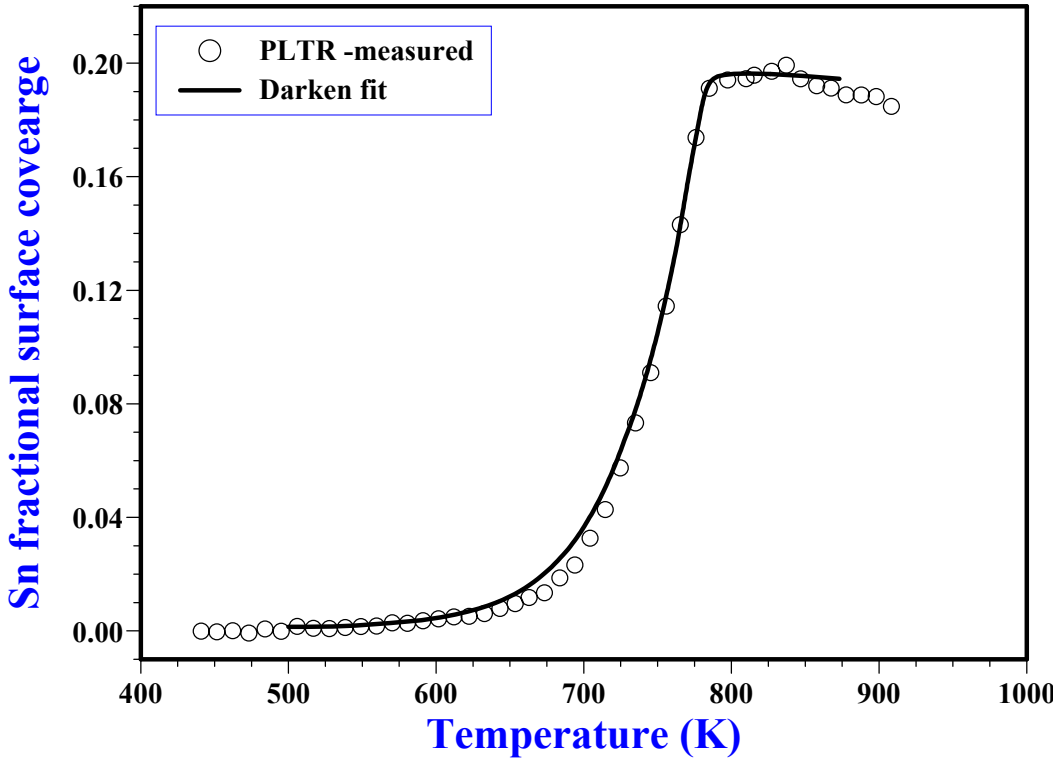

Figure 4.4 Measured Sn segregation in Cu(100) for PLTR run at heating rate of 0.075 K/s and the Darken model fit for segregation parameters: D_o = 6.2 × 10^{-6} m^2/s, E = 189 kJ/mol, ΔG = 65 kJ/mol and Ω_{CuSn} = 3.8 kJ/mol.

c) Sample heating rate: 0.15 K/s

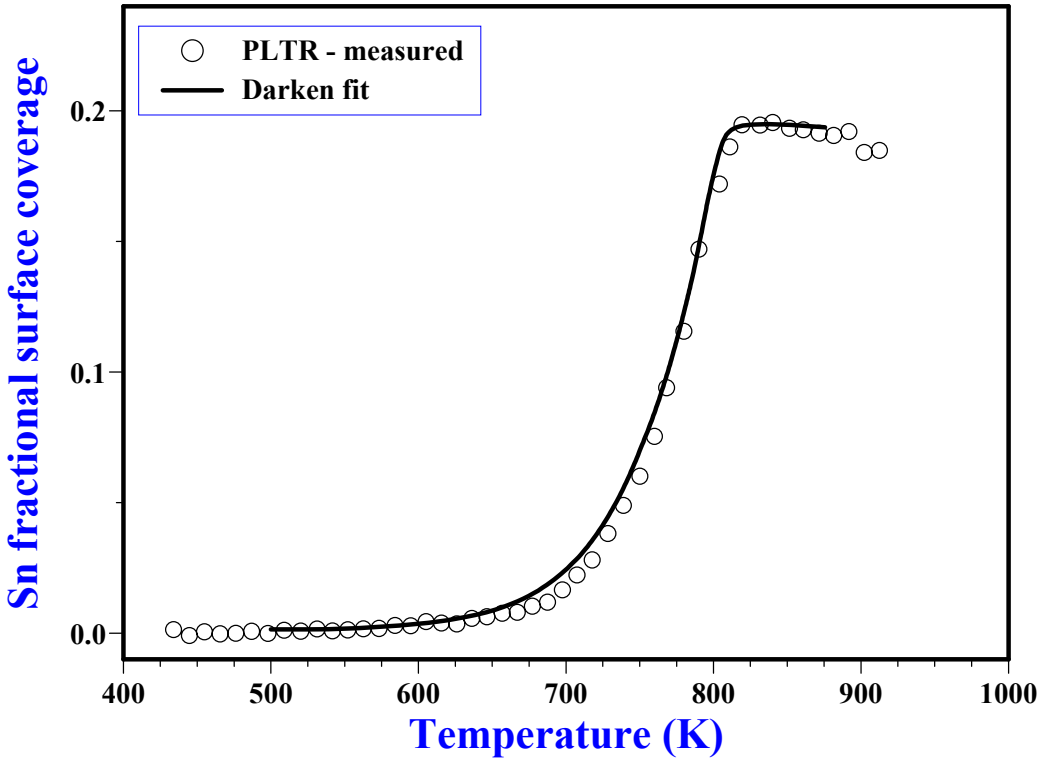

Figure 4.5 Measured Sn segregation in Cu(100) for PLTR run at heating rate of 0.15 K/s and the Darken model fit for segregation parameters: D_o = 5.8 × 10^{-6} m^2/s, E = 190 kJ/mol, ΔG = 65 kJ/mol and Ω_{CuSn} = 4.0 kJ/mol.

For the rest of the results involving Cu(110)Sn and Cu(111)Sn, the fit from the auxiliary models of Fick and Bragg-Williams were combined on the same system of axes and considered only for rates of ± 0.05 K/s. The main modified Darken model were however used to fit three different rates for each of the two orientations.

4.2.2 Cu(110)Sn binary system

4.2.2.1 The Fick integral and Bragg-Williams fits

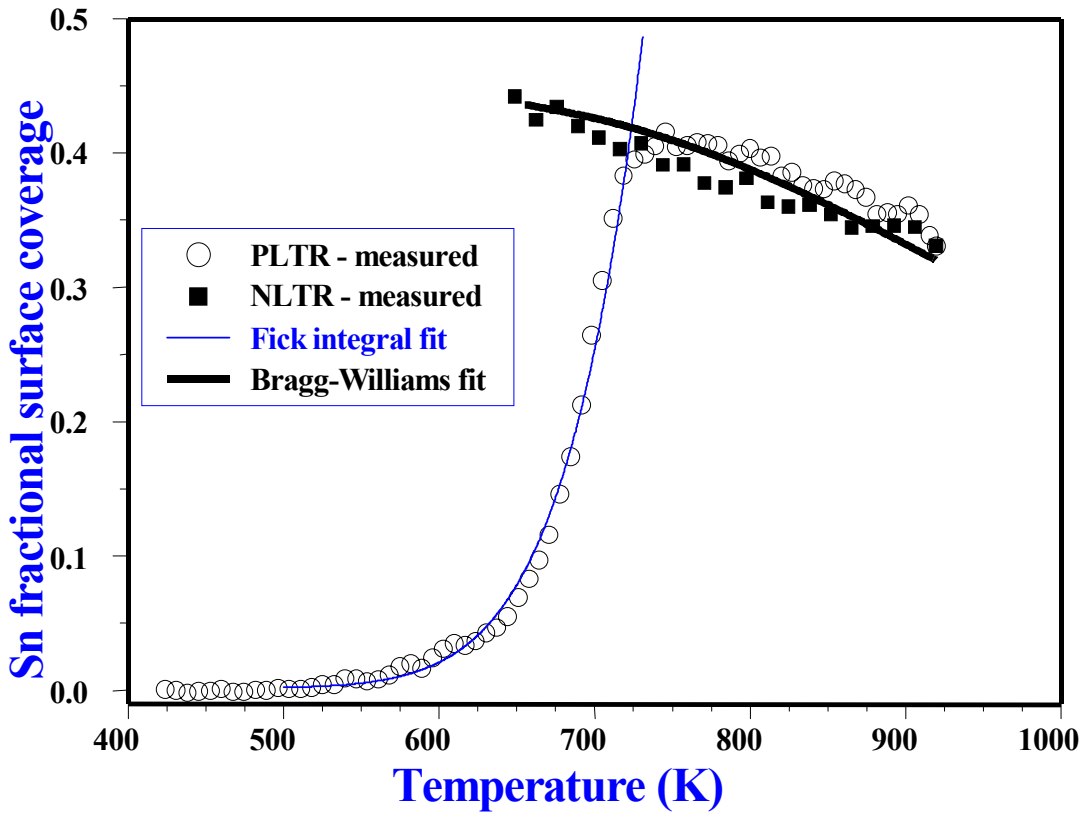

Figure 4.6 Measured Sn segregation in Cu(110) for PLTR and NLTR runs at heating rate and cooling rates of ± 0.05 K/s respectively as well as the calculated Fick integral equation (D_o = 2.8 × 10^{-6} m^2/s and E = 168 kJ/mol) and the calculated Bragg-Williams equation (ΔG = 62 kJ/mol and Ω_{CuSn} = 3.8 kJ/mol.).

4.2.2.2 The modified Darken fits

a) Sample heating rate: 0.05 K/s

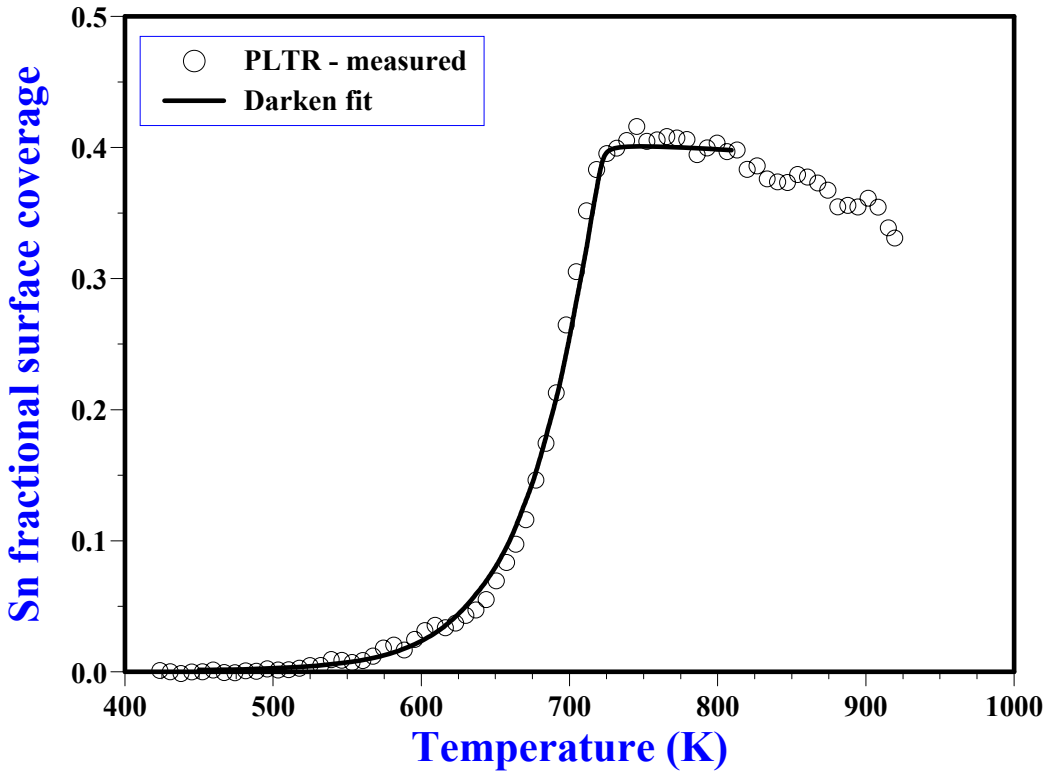

Figure 4.7 Measured Sn segregation in Cu(110) for PLTR run at heating rate of 0.05 K/s and the Darken model fit for segregation parameters: D_o = 2.8 × 10^{-6} m^2/s, E = 168 kJ/mol, ΔG = 62 kJ/mol and Ω_{CuSn} = 3.8 kJ/mol.

b) Sample heating rate: 0.075 K/s

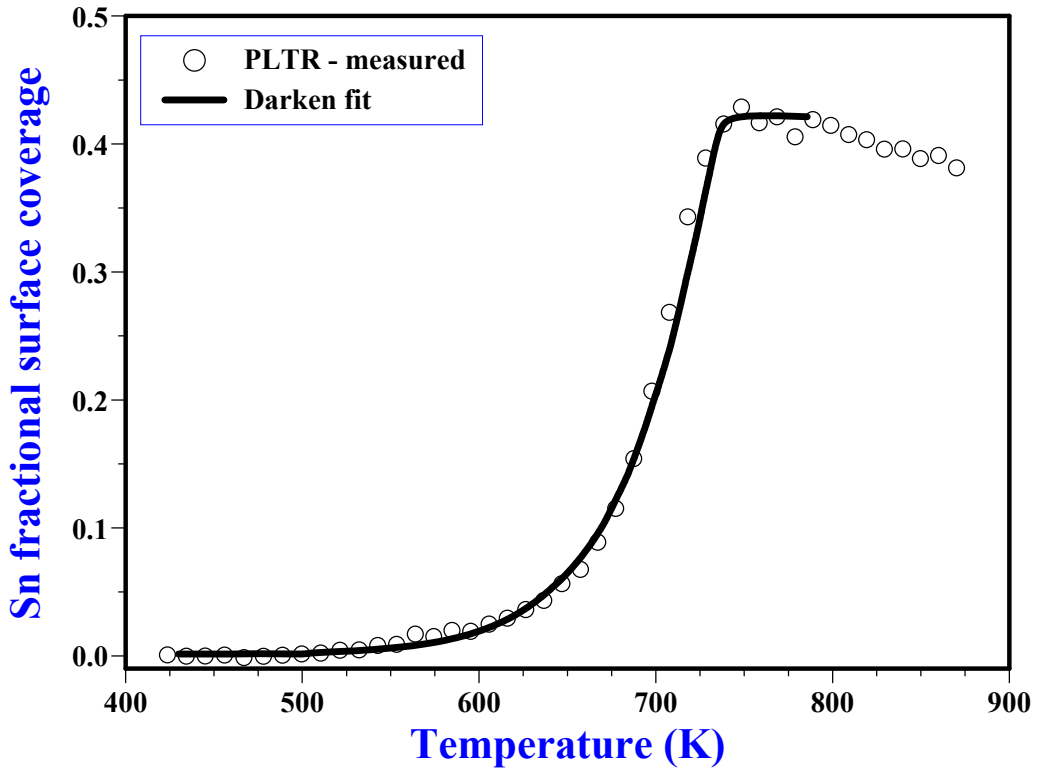

Figure 4.8 Measured Sn segregation in Cu(110) for PLTR run at heating rate of 0.075 K/s and the Darken model fit for segregation parameters: D_o = 2.9 × 10^{-6} m^2/s, E = 168 kJ/mol, ΔG = 62 kJ/mol and Ω_{CuSn} = 3.8 kJ/mol.

c) Sample heating rate: 0.15 K/s

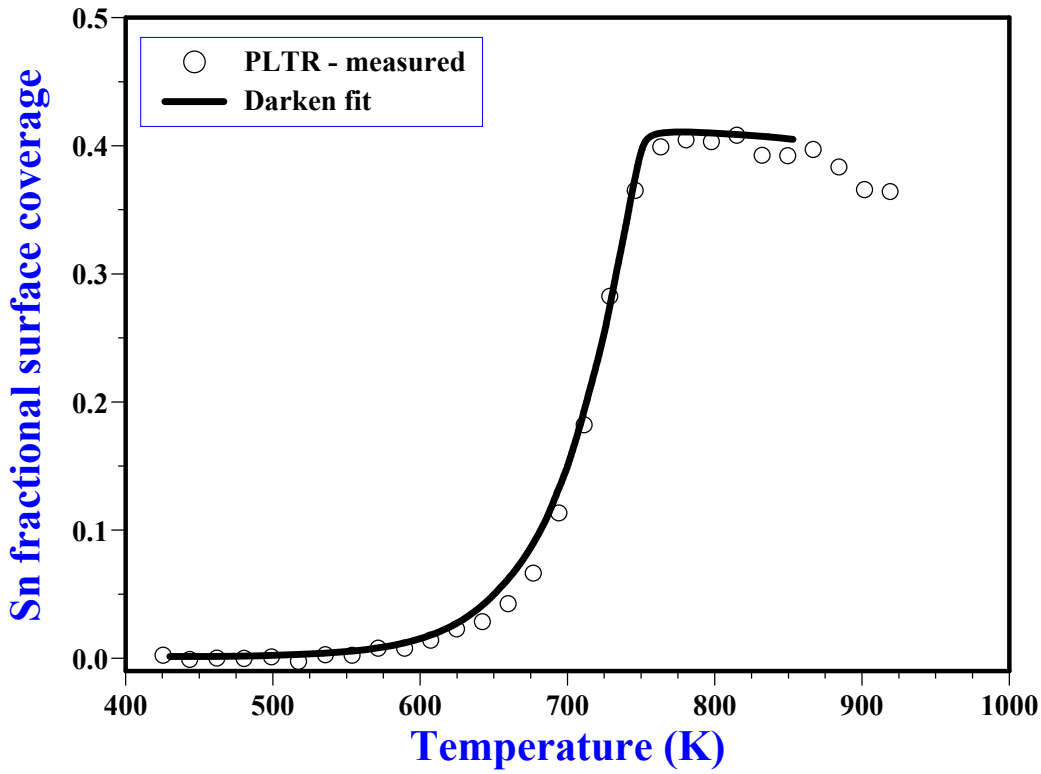

Figure 4.9 Measured Sn segregation in Cu(110) for PLTR run at heating rate of 0.15 K/s and the Darken model fit for segregation parameters: D_o = 2.9 × 10^{-6} m^2/s, E = 168 kJ/mol, ΔG = 63 kJ/mol and Ω_{CuSn} = 3.8 kJ/mol.

4.2.3 Cu(111)Sn binary system

4.2.3.1 The Fick integral and Bragg-Williams fits

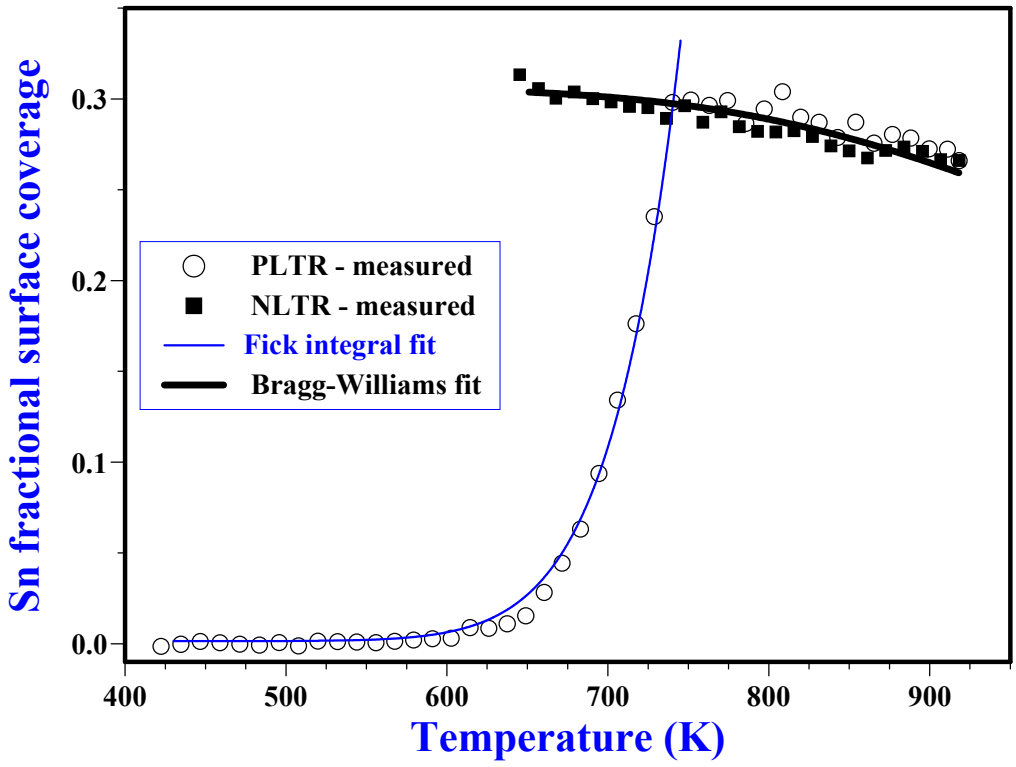

Figure 4.10 Measured Sn segregation in Cu(111) for PLTR and NLTR runs at heating rate and cooling rates of ± 0.05 K/s respectively as well as the calculated Fick integral equation (D_o = 9.2 × 10^{-4} m^2/s and E = 205 kJ/mol) and the calculated Bragg-Williams equation (ΔG = 69 kJ/mol and Ω_{CuSn} = 3.8 kJ/mol.).

4.2.3.2 The modified Darken fits

a) Sample heating rate: 0.05 K/s

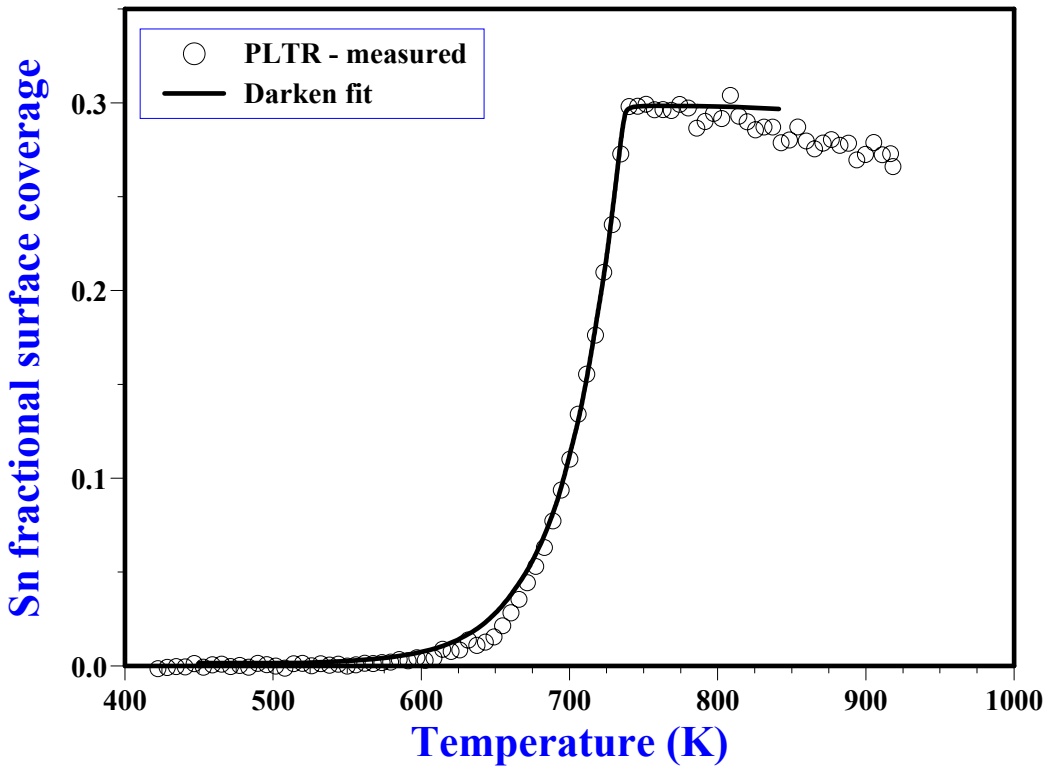

Figure 4.11 Measured Sn segregation in Cu(111) for PLTR run at heating rate of 0.05 K/s and the Darken model fit for segregation parameters: D_o = 9.2 × 10^{-4} m^2/s, E = 205 kJ/mol, ΔG = 70 kJ/mol and Ω_{CuSn} = 3.8 kJ/mol.

b) Sample heating rate: 0.075 K/s

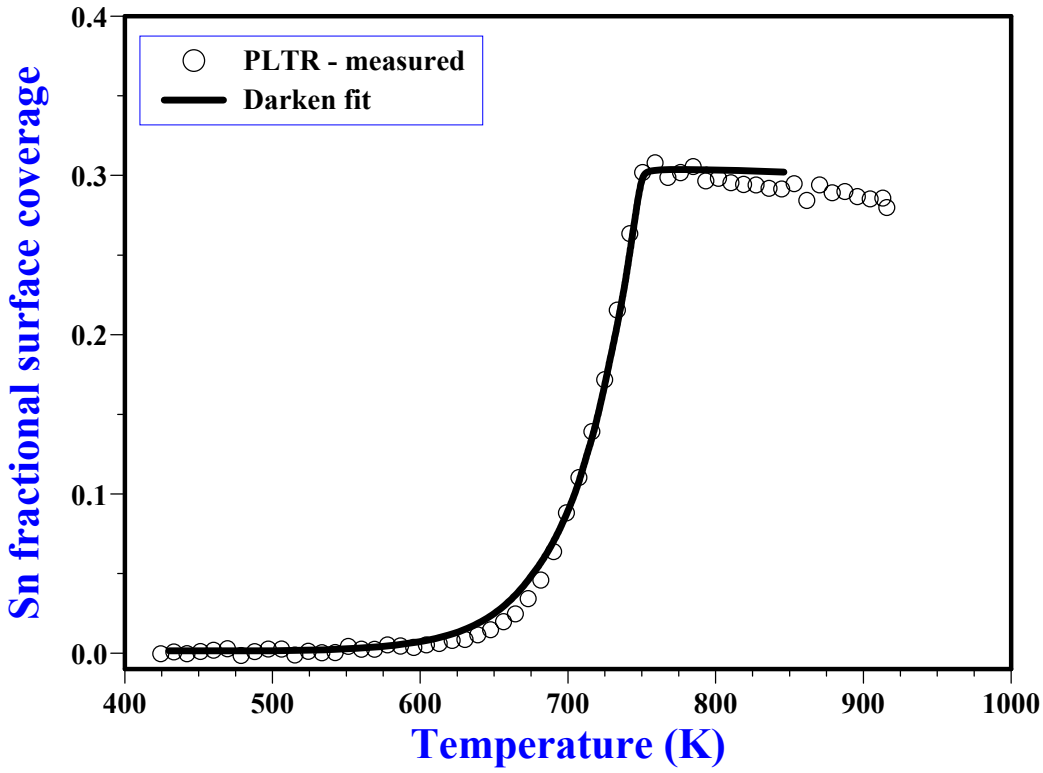

Figure 4.12 Measured Sn segregation in Cu(111) for PLTR run at heating rate of 0.075 K/s and the Darken model fit for segregation parameters: D_o = 9.2×10^{-4} m^2/s, E = 205 kJ/mol, ΔG = 69 kJ/mol and Ω_{CuSn} = 3.8 kJ/mol.

c) Sample heating rate: 0.10 K/s

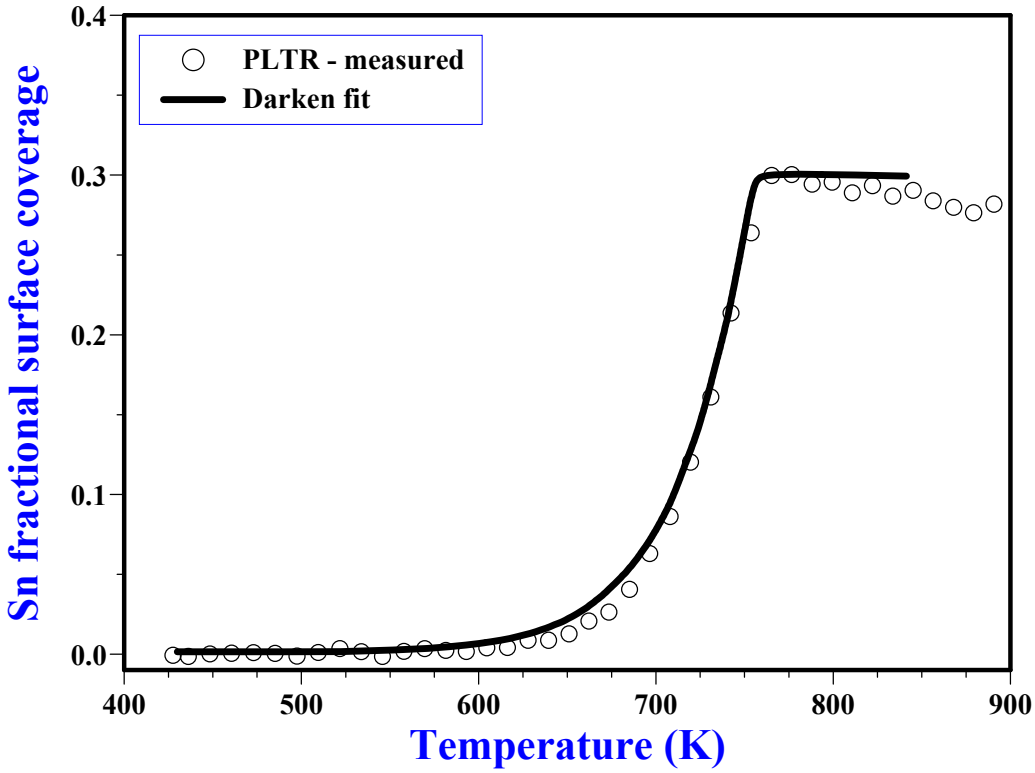

Figure 4.13 Measured Sn segregation in Cu(111) for PLTR run at heating rate of 0.10 K/s and the Darken model fit for segregation parameters: D_o = 9.2 × 10^{-4} m^2/s, E = 205 kJ/mol, ΔG = 69 kJ/mol and Ω_{CuSn} = 3.8 kJ/mol.

4.2.4 A summary of Sn segregation parameters in CuSn binary alloy

Orientation	Rate (K/s)	D_o (± 5%) (m^2/s)	E (± 1) (kJ/mol)	ΔG (± 1) (kJ/mol)	Ω_{CuSn} (± 0.2) (kJ/mol)
Cu(100)	0.050	6.2×10^{-6}	189	65	3.9
	0.075	6.2×10^{-6}	189	65	3.8
	0.150	5.8×10^{-6}	190	65	4.0
Cu(110)	0.050	2.7×10^{-6}	168	62	3.8
	0.075	2.9×10^{-6}	168	62	3.8
	0.150	2.8×10^{-6}	168	63	3.8
Cu(111)	0.050	9.2×10^{-4}	205	70	3.8
	0.075	9.2×10^{-4}	205	69	3.8
	0.100	9.2×10^{-4}	205	69	3.8

Table 4.1. The segregation parameters of Sn in Cu(100), Cu(110) and Cu(111). The errors indicated in the top row were not calculated statistically, but guessed from a change in the fit profile for a certain change in the specific segregation parameter.

4.3 The ternary Cu-Sn-Sb system

The solution of the Guttman equations was done using a MATLAB mathematical fitting routine, *fmins* based on Nelder-Mead Simplex Algorithm [77]. The equations were used to fit the experimental data for the NLTR runs. See **Appendix A** for the flow chart. Segregation parameters from the Guttman fits were then used as starting parameters in the main model, the modified Darken equations.

4.3.1 Cu(100)SnSb ternary system

4.3.1.1 Guttman fits

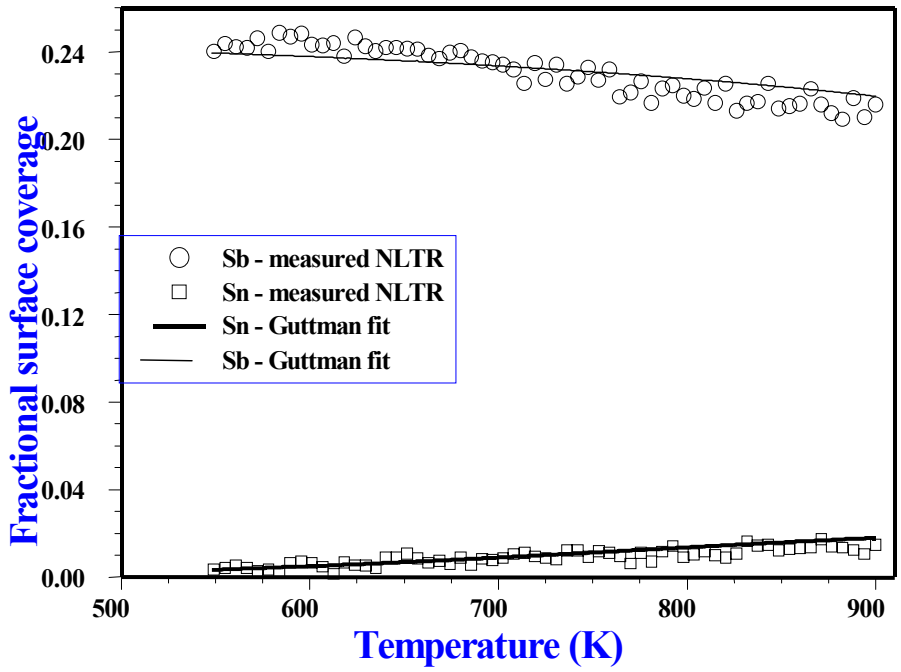

Figure 4.14 Measured Sn and Sb segregation in Cu(100) from NLTR run at –0.05 K/s. --

Calculated solid lines are fits using **equations 2.29** to **2.32** with ΔG_{Sn} = 66 kJ/mol, ΔG_{Sb} = 83 kJ/mol, Ω_{CuSn} = 3.4 kJ/mol, Ω_{CuSb} = 15.9 kJ/mol and Ω_{SnSb} = - 5.4 kJ/mol.

The energetic segregation parameters are the same, for a particular crystal orientation, irrespective of the sample "low" cooling rates for the profiles obtained from the equilibrium segregation runs (NLTR). These five segregation parameters, obtained from the Guttman fits were then introduced as starting fit values in the modified Darken model. The other remaining starting parameters are the four from the kinetics segregation region, the D_o and E's, and these were chosen from the binary alloy values.

4.3.1.2 The modified Darken fits

a) Sample heating rate: 0.05 K/s

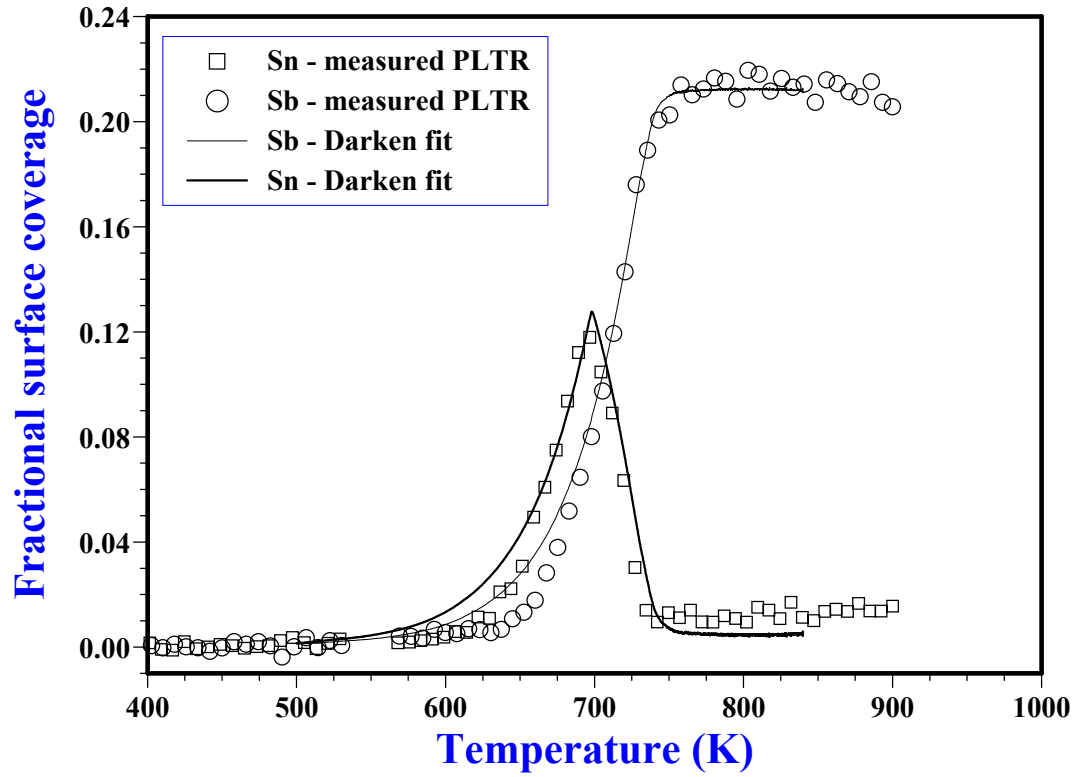

Figure 4.15 Measured Sn and Sb segregation in Cu(100) for a PLTR run at a rate of 0.05 K/s and the modified Darken model calculations for segregation parameters: $D_{o(Sn)} = 6.3 \times 10^{-6}$ m^2/s, $D_{o(Sb)} = 2.8 \times 10^{-5}$ m^2/s, $E_{Sn} = 175$ kJ/mol, $E_{Sb} = 186$ kJ/mol, $\Delta G_{Sn} = 65$ kJ/mol, $\Delta G_{Sb} = 84$ kJ/mol, $\Omega_{CuSn} = 3.4$ kJ/mol, $\Omega_{CuSb} = 15.9$ kJ/mol and $\Omega_{SnSb} = -5.4$ kJ/mol.

b) Sample heating rate: 0.075 K/s

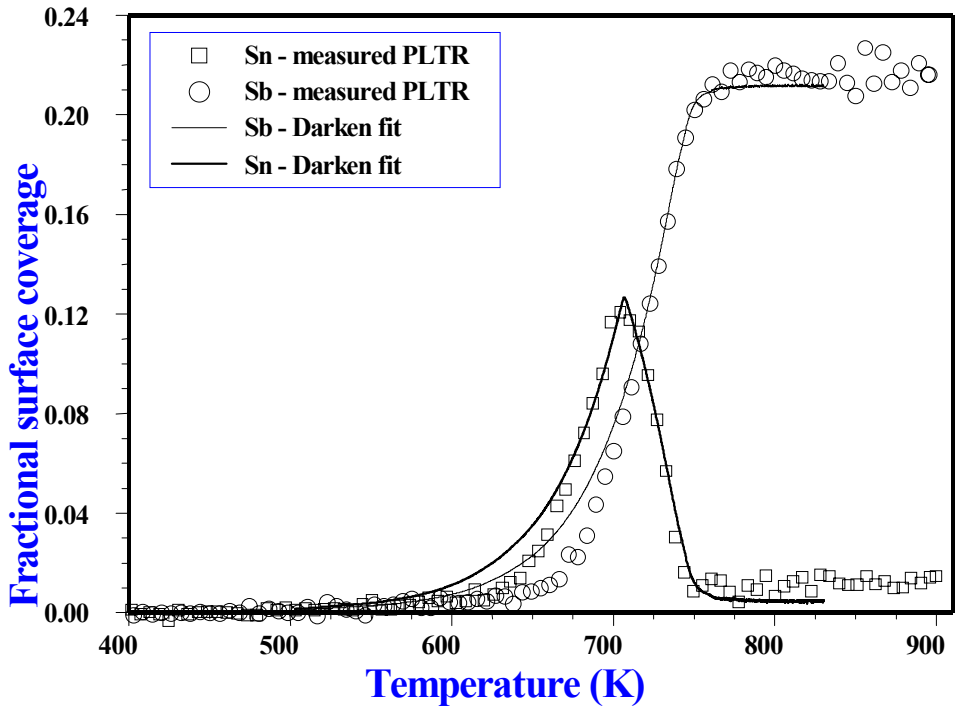

Figure 4.16 Measured Sn and Sb segregation in Cu(100) for PLTR run and the Darken model calculations for segregation parameters: $D_{o(Sn)}$ = 6.3 × 10^{-6} m^2/s, $D_{o(Sb)}$ = 2.8×10^{-5} m^2/s, E_{Sn} = 175 kJ/mol, E_{Sb} = 186 kJ/mol, ΔG_{Sn} = 64 kJ/mol, ΔG_{Sb} = 84 kJ/mol, Ω_{CuSn} = 3.4 kJ/mol, Ω_{CuSb} = 15.9 kJ/mol and Ω_{SnSb} = -5.4 kJ/mol.

c) Sample heating at 0.15 K/s

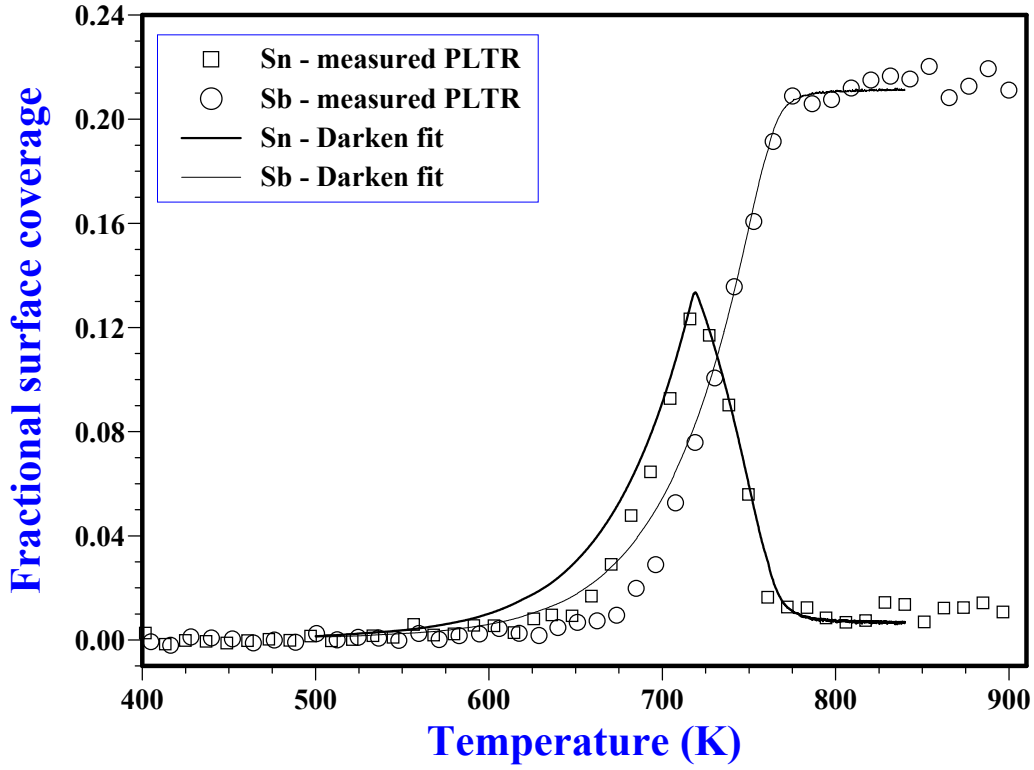

Figure 4.17 Measured Sn and Sb segregation in Cu(100) for PLTR run and the modified Darken model calculations for segregation parameters: $D_{o(Sn)}$ = 6.3 × 10^{-6} m^2/s, $D_{o(Sb)}$ = 2.8×10^{-5} m^2/s, E_{Sn} = 175 kJ/mol, E_{Sb} = 186 kJ/mol, ΔG_{Sn} = 65 kJ/mol, ΔG_{Sb} = 84 kJ/mol, Ω_{CuSn} = 3.4 kJ/mol, Ω_{CuSb} = 15.9 kJ/mol and Ω_{SnSb} = -5.1 kJ/mol.

The modified Darken fits in the temperature region of 580 to 705 K for **figures 4.15** to **4.17** are not good. This is perhaps experimental procedure problem due to the depleted, non-equilibrium near surface region, brought about as a result of the Ar^+ ion sputtering of the sample surface prior to the segregation run. This procedure is unfortunately unavoidable.

4.3.2 Cu(111)SnSb ternary system

4.3.2.1 Guttman fits

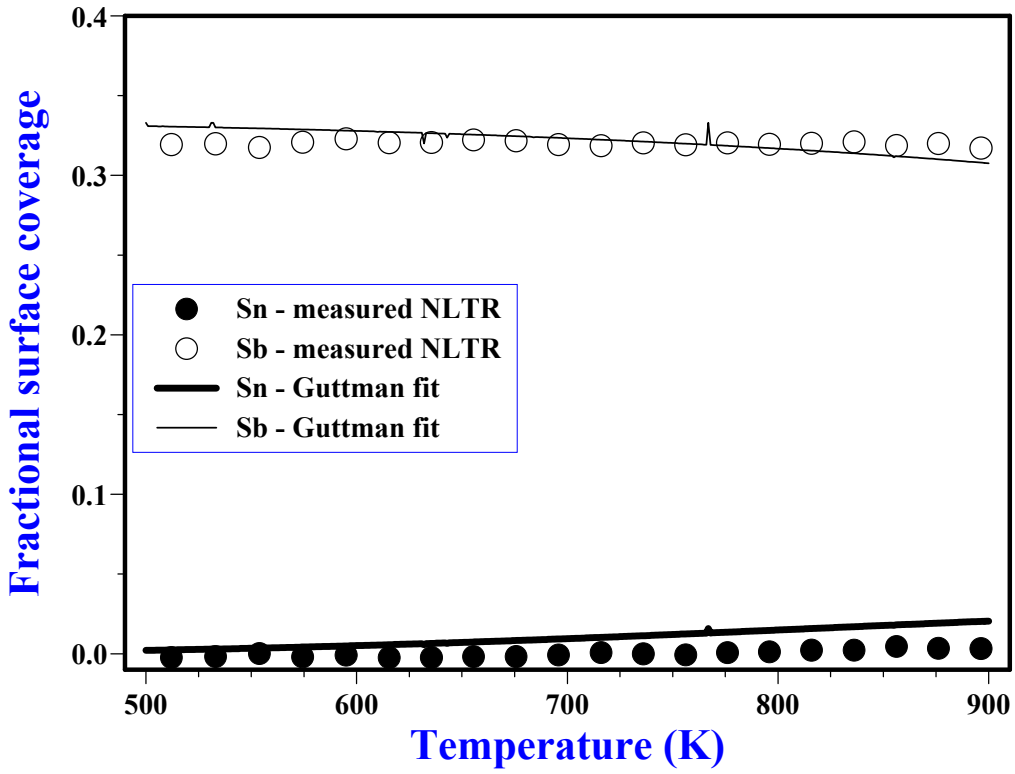

Figure 4.18 Measured Sn and Sb segregation in Cu(111) from NLTR run at – 0.05 K/s. Calculated solid lines are the Guttman's fit for ΔG_{Sn} = 68 kJ/mol, ΔG_{Sb} = 86 kJ/mol, Ω_{CuSn} = 3.6 kJ/mol, Ω_{CuSb} = 16.2 kJ/mol and Ω_{SnSb} = - 5.3 kJ/mol.

The above energetic parameters were then used as starting values in the modified Darken equations.

4.3.2.2 The modified Darken fits

a) Sample heating rate: 0.05 K/s

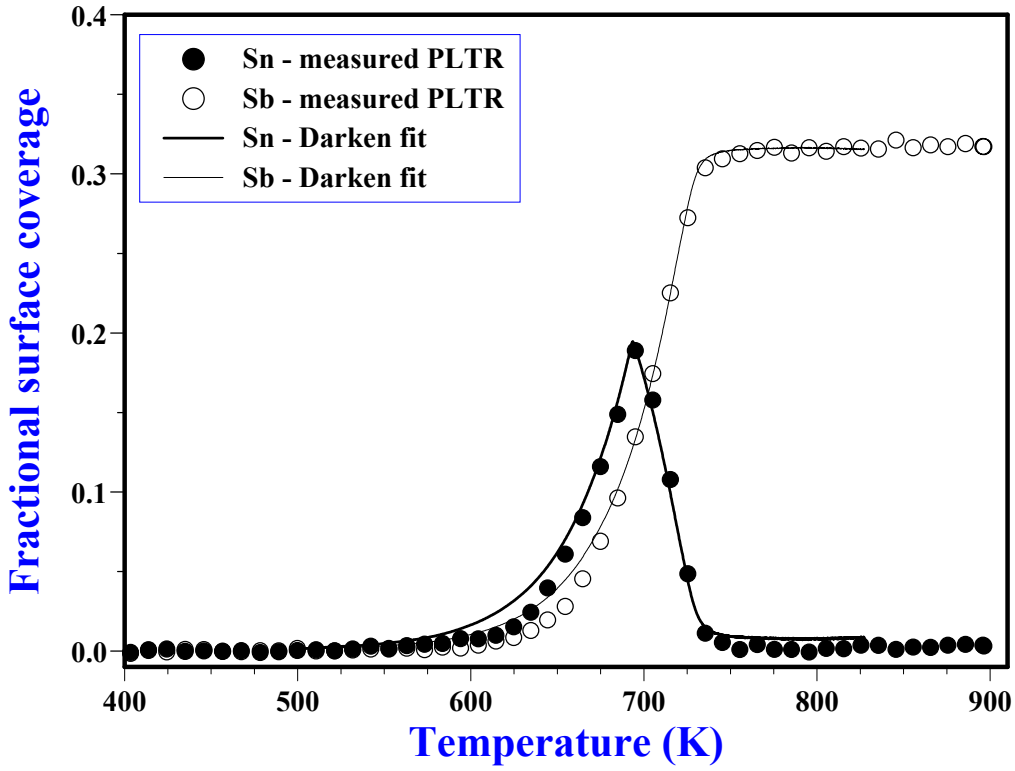

Figure 4.19 Measured Sn and Sb segregation in Cu(111) for PLTR run and the Darken model calculations for segregation parameters: $D_{o(Sn)} = 9.3 \times 10^{-4}$ m^2/s, $D_{o(Sb)} = 3.4 \times 10^{-3}$ m^2/s $E_{Sn} = 196$ kJ/mol, $E_{Sb} = 206$ kJ/mol, $\Delta G_{Sn} = 68$ kJ/mol, $\Delta G_{Sb} = 86$ kJ/mol, $\Omega_{CuSn} = 3.6$ kJ/mol, $\Omega_{CuSb} = 16.2$ kJ/mol and $\Omega_{SnSb} = -5.3$ kJ/mol.

b) Sample heating at 0.075 K/s

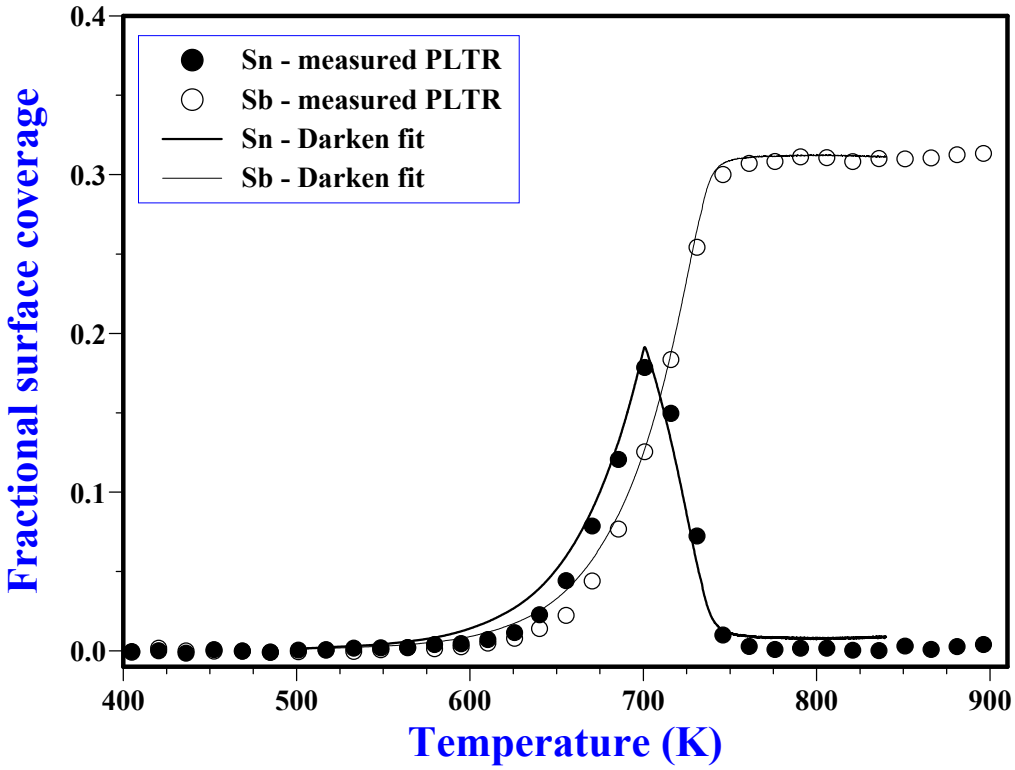

Figure 4.20 Measured Sn and Sb segregation in Cu(111) for PLTR run and the Darken model calculations for segregation parameters: $D_{o(Sn)} = 9.3 \times 10^{-4}$ m^2/s, $D_{o(Sb)} = 3.4 \times 10^{-3}$ m^2/s, $E_{Sn} = 196$ kJ/mol, $E_{Sb} = 206$ kJ/mol, $\Delta G_{Sn} = 68$ kJ/mol, $\Delta G_{Sb} = 86$ kJ/mol, $\Omega_{CuSn} = 3.6$ kJ/mol, $\Omega_{CuSb} = 16.2$ kJ/mol and $\Omega_{SnSb} = -5.3$ kJ/mol.

c) Sample heating at 0.15 K/s

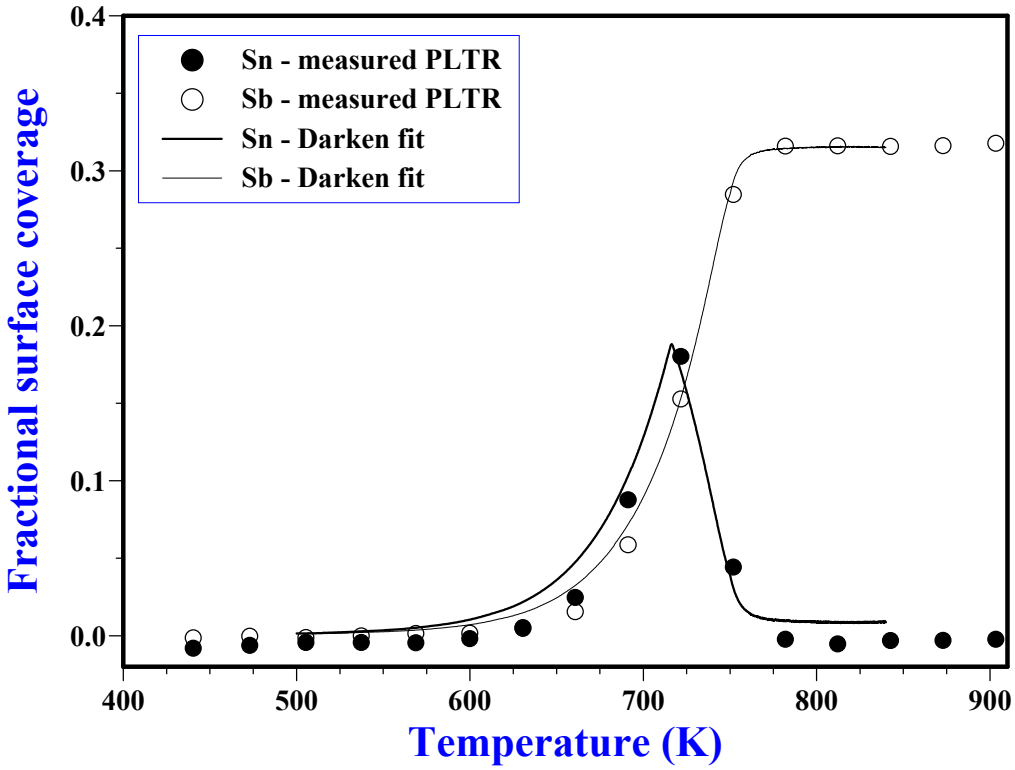

Figure 4.21 Measured Sn and Sb segregation in Cu(111) for PLTR run and the Darken model calculations for segregation parameters: $D_{o(Sn)} = 9.1 \times 10^{-4}$ m^2/s, $D_{o(Sb)} = 3.4 \times 10^{-3}$ m^2/s, $E_{Sn} = 196$ kJ/mol, $E_{Sb} = 206$ kJ/mol, $\Delta G_{Sn} = 68$ kJ/mol, $\Delta G_{Sb} = 86$ kJ/mol, $\Omega_{CuSn} = 3.6$ kJ/mol, $\Omega_{CuSb} = 16.2$ kJ/mol and $\Omega_{SnSb} = -5.3$ kJ/mol.

4.3.3 A summary of Sn and Sb segregation parameters in Cu(100) and Cu(111).

Crystal	Segregating Species	Rate (K/s)	D_0 (± 5%) (m^2/s)	E (± 1) (kJ/mol)	ΔG (± 1) (kJ/mol)	$\Omega_{Cu\text{-}i}$ (± 0.2) (kJ/mol)	Ω_{SnSb} (± 0.3) (kJ/mol)
Cu(100)	Sn	0.05	6.3×10^{-6}	175	65	3.4	- 5.4
		0.075	6.3×10^{-6}	175	64	3.4	
		0.15	6.3×10^{-6}	175	65	3.4	
	Sb	0.05	2.8×10^{-5}	186	84	15.9	
		0.075	2.8×10^{-5}	186	84	15.9	
		0.15	2.8×10^{-5}	186	84	15.9	
Cu(111)	Sn	0.05	9.3×10^{-4}	196	68	3.6	- 5.3
		0.075	9.3×10^{-4}	196	68	3.6	
		0.15	9.1×10^{-4}	196	68	3.6	
	Sb	0.05	3.4×10^{-3}	206	86	16.2	
		0.075	3.4×10^{-3}	206	86	16.2	
		0.15	3.4×10^{-3}	206	86	16.2	

Table 4.2. The segregation parameters of Sn and Sb in Cu(100) and Cu(111).

The average segregation parameters in **Tables 4.1** and **4.2** will be used in the discussion chapter that follows.

CHAPTER FIVE

DISCUSSIONS AND CONCLUSIONS

5.1 Introduction

The discussions will follow the sequence as given in **Section 4.1** in **Chapter Four**. The segregation of solute Sn in the binary CuSn will be considered first and will be followed by discussions on Sn and Sb in the ternary CuSnSb system. Both Sn and Sb segregation profiles in the two orientations, namely Cu(100) and Cu(111) will be compared. Finally, the progression study of Sn segregation in both binary and ternary systems will then be discussed.

5.2 The binary Cu-Sn system

Sn has a larger atomic size than Cu. This size mismatch causes a lattice strain distortion that can only be minimized by the creation of vacancy-solute atom association. There is also the electronic factor due to the differences in valency between the solute Sn and the solvent Cu atoms. Vacancies in pure metals tend to have a negative electrical character, and are hence attracted to regions wherein the localized electron density is less than that of the matrix average [78]. A quadrivalent Sn will interact with the negatively charged vacancy by the electrostatic screened Coulomb attraction. As a result of this binding energy, the vacancy formation energy is reduced and the vacancy concentration is enhanced. This enhances solute Sn segregation in the sense that a diffusive jump occurs only via an exchange of position with an adjacent vacancy [79]. This behaviour of Sn, among others, is seen in the following segregation profiles.

5.2.1. Sn segregation profile in Cu single crystal

Following the method of PLTR, four main regions could be identified from the Sn segregation profile in **figure 5.1**. In the region below the temperature line A, the temperature is low and therefore the diffusion coefficient *D* is small. However, the small surface concentration detected by the AES system, and called the surface dumping effect, is caused by the segregation energy.

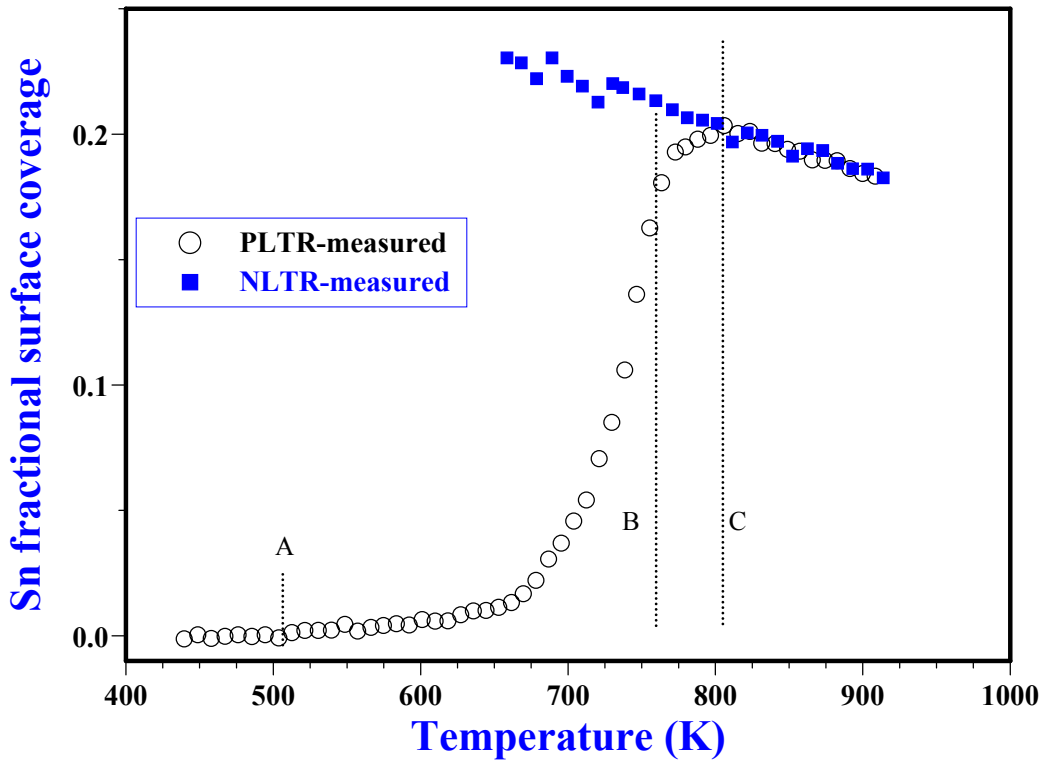

Figure 5.1 A typical measured Sn segregation profile in Cu(100) for both PLTR at 0.05 K/s and NLTR at –0.05 K/s showing the kinetic as well as the equilibrium segregation regions.

As the temperature increases, however, the bulk diffusion becomes the dominating effect. *D* values of the segregating species increase and the flux of Sn atoms increase from the bulk to the surface. These occurrences give the kinetic segregation region profile identified to be between the temperature lines A and B. The Fick integral was used to fit some of the data points in this region to yield the bulk diffusion parameters of D_o and E. (See **figure 4.1**). The region between the temperature lines B and C is governed by the differences in the chemical potential energy ($\Delta\mu$) between the layers that are now rapidly decreasing and are approaching zero. The next region could be identified as the equilibrium region, govern by the saturation effect [80] where $\Delta\mu = 0$ and for the PLTR,

is identified as the narrow region above the temperature line C. In this region, the diffusion coefficient is large enough for a quasi-equilibrium description of the segregation process.

Immediately after the PLTR run, the sample could be cooled linearly with time to give the negative linear temperature ramp (NLTR) profile. **Figure 5.1** clearly shows that all the data points from the NLTR runs follow after the equilibrium section of PLTR. One could assert therefore that the equilibrium section of the PLTR run is extended be employing the NLTR run. The NLTR region is further confirmed as equilibrium region with a repeat of PLTR run immediately after the NLTR run. The advantage of the NLTR runs is that the equilibrium region is now extended and well defined and the use of the Bragg-Williams equation to fit the experimental data points will yield a more unique set of Ω_{12} and ΔG values than would be the case had the equilibrium section of the PLTR run only been used [81].

The role of the different heating and cooling rates are now visited in relation to Sn segregation in the three single Cu crystals. **Figures 5.2**, **5.3** and **5.4** portray Sn segregation profiles in Cu(100), Cu(110) and Cu(111) respectively. Each profile consists of the combination of PLTR and NLTR runs for a particular heating cum cooling rates.

5.2.2 Sn segregation profile at different rates

5.2.2.1 Sn in Cu(100)

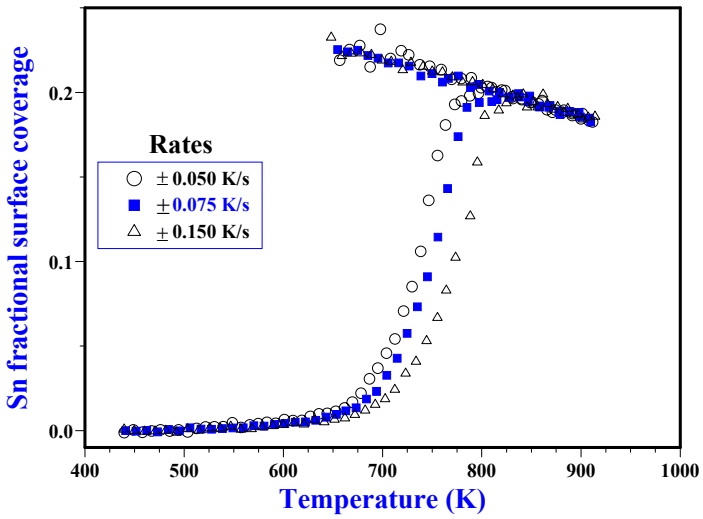

Figure 5.2 Measured Sn segregation profiles in Cu(100) at different heating rates

5.2.2.2 Sn in Cu(110)

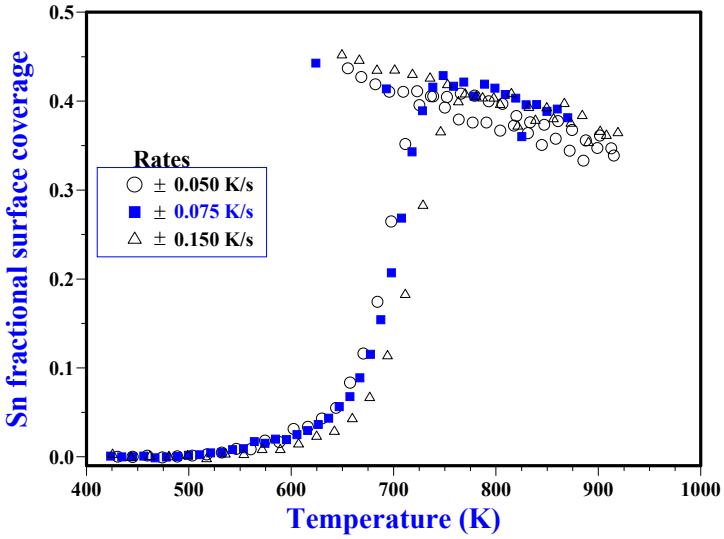

Figure 5.3 Measured Sn segregation profiles in Cu(110) at different heating rates

5.2.2.3 Sn in Cu(111)

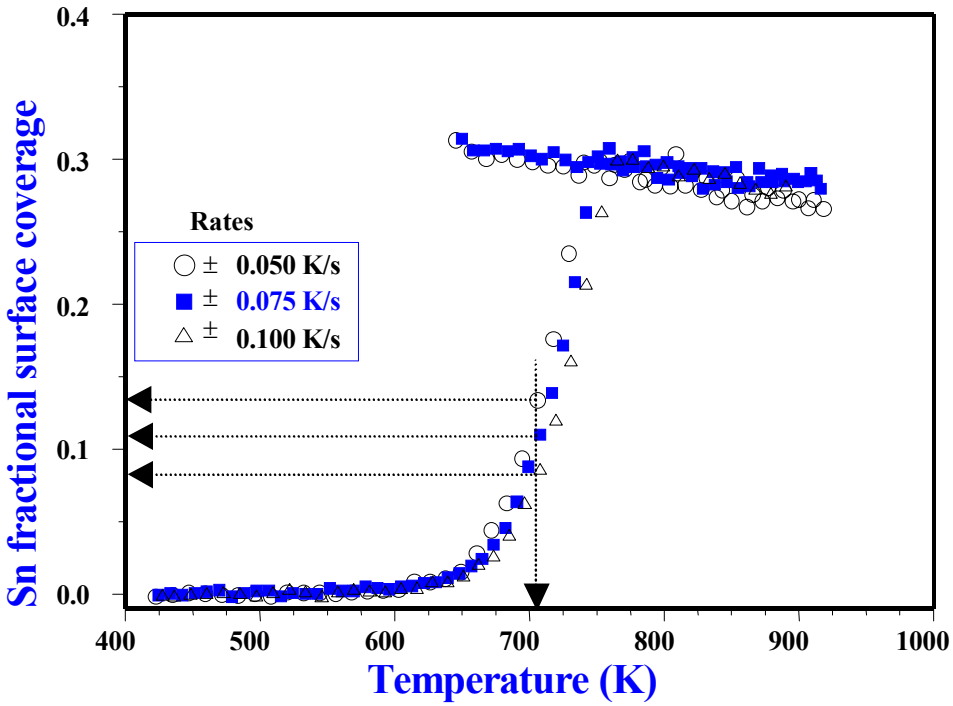

Figure 5.4 Measured Sn segregation profiles in Cu(111) at different heating rates

The segregation profiles of Sn in **figures 5.2**, **5.3** and **5.4**, in the three low index planes of Cu show the same trend. Firstly, the curves shift to higher temperatures as the rate of heating the sample increases. Viljoen and du Plessis [82] have also observed these shifts. At a particular temperature in the kinetic region of the segregation profile, say 705 K, as indicated in **figure 5.4**, a higher Sn coverage is seen on the surface for the slowest heating rate because the Sn atoms have had much more time to diffuse from the bulk to the surface at that temperature. Secondly, for each of the Cu crystals, Sn segregation profiles (NLTR) obtained during cooling from high temperatures are within experimental error, the same irrespective of the "low" cooling rates. This confirms the NLTR profiles to be equilibrium profiles.

The next step in looking at the behaviour of Sn in binary CuSn alloy is to compare its segregation function in all three orientations at a particular heating and cooling rate.

5.2.3 Sn segregation profile in the three low index planes of Cu at the same rate

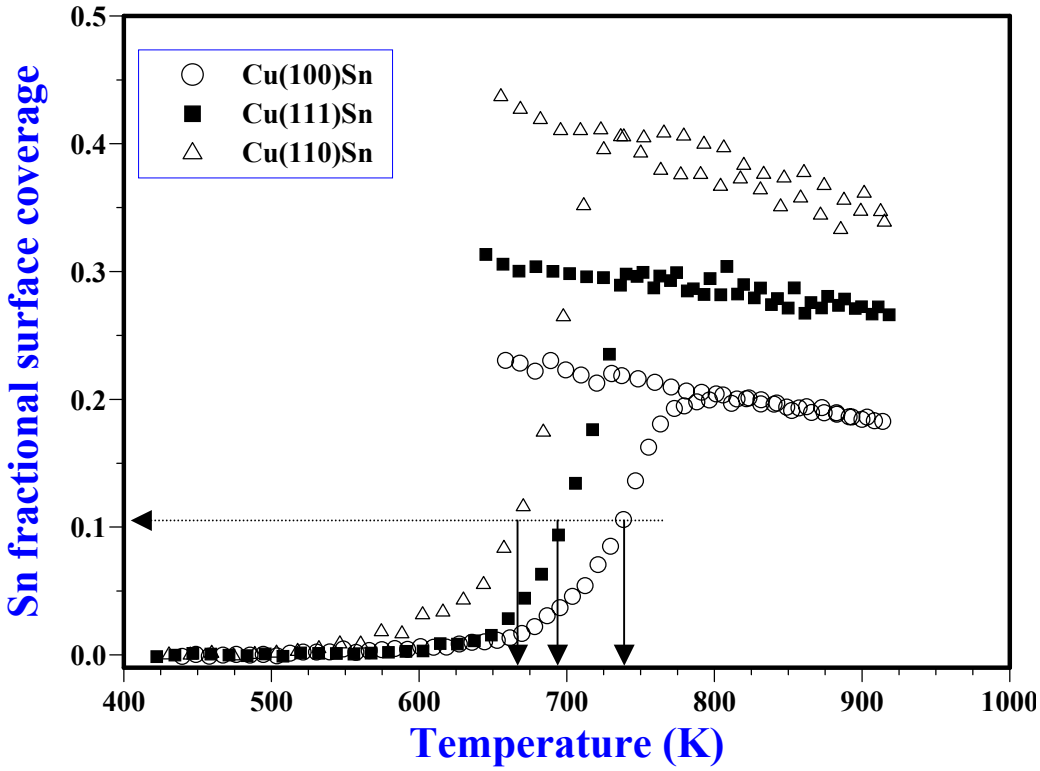

Figure 5.5 Measured Sn segregation profiles in the three different Cu orientations at rates of ± 0.05 K/s

The temperature at which the Sn surface concentration reaches, say 0.1 at.%, in **figure 5.5**, is different for the different crystal orientations. In Cu(110) the temperature is 669 K while that for Cu(111) and Cu(100) are 694 K and 740 K respectively. This indicates

different Sn diffusion rates for the different orientations. These different Sn segregation behaviours could be attributed to the number of vacancies that exist in the topmost layers. For the different Cu orientations, the number of vacancies and their corresponding vacancy formation energies are not the same. An atom within the bulk has a coordination number of 12. However, once it makes its way to the surface it has a new coordination number in relation to its Cu neighbouring atoms. A surface impurity atom on Cu(110), Cu(100) and Cu(111) surfaces bonds with five, four and three nearest-neighbour Cu atoms, respectively. The surface cohesion energies, accordingly, is highest for Cu(110) and least for Cu(111) [83]. A similar surface energy trend was found for Pd, another fcc metal [84]. The vacancy formation energy can be defined as the difference between the bulk cohesion energy and the surface cohesion energy. Thus, Cu(110) has the lowest vacancy formation energy, followed by Cu(100) while Cu(111) has the highest [85]. But the activation energy of diffusion in the bulk is the sum of the migration energy and the vacancy formation energy [86]. Flynn [87] has calculated the migration energy of a Cu atom in the bulk as 80.9 kJ/mol. It is to be expected, therefore, that the activation energies (E_i) of a migrating atom in the different Cu orientations would differ because of the different vacancy formation energies, and these would indeed affect the diffusion rates accordingly. Migrating atoms in a Cu(110) crystal will have the highest diffusion rate. The E values from **Table 4.1** are repeated here as: $E_{Sn(110)}$ = 167.8 kJ/mol, : $E_{Sn(100)}$ = 189.4 kJ/mol and : $E_{Sn(111)}$ = 204.6 kJ/mol and they confirm the above fact that the diffusion rate of Sn in Cu(110) is the highest.

However, from **figures 5.5** and **5.6**, it is established that the migrating atoms in Cu(111) have a higher diffusion rate than in Cu(100). It is to be expected then that the pre-exponential factor D_o (which consists of the frequency of vibration of the impurity atom

about its lattice position, the jump distance to a vacancy and an entropy of activation term) in Cu(111) would be higher than in Cu(100). Actually, $D_{o(111)}$ is two orders of magnitude higher than $D_{o(100)}$ The quantified values from **Table 4.1** are: $D_{o(111)} = 9.2 \times 10^{-4}$ m^2/s and $D_{o(100)} = 6.1 \times 10^{-6}$ m^2/s and these justify the fact that Sn in Cu(111) segregation profile will lie at lower temperatures as compared to Cu(100). The other result for heating and cooling rates of ± 0.075 K/s is shown in **figure 5.6**. It shows similar trends for the different Cu orientations.

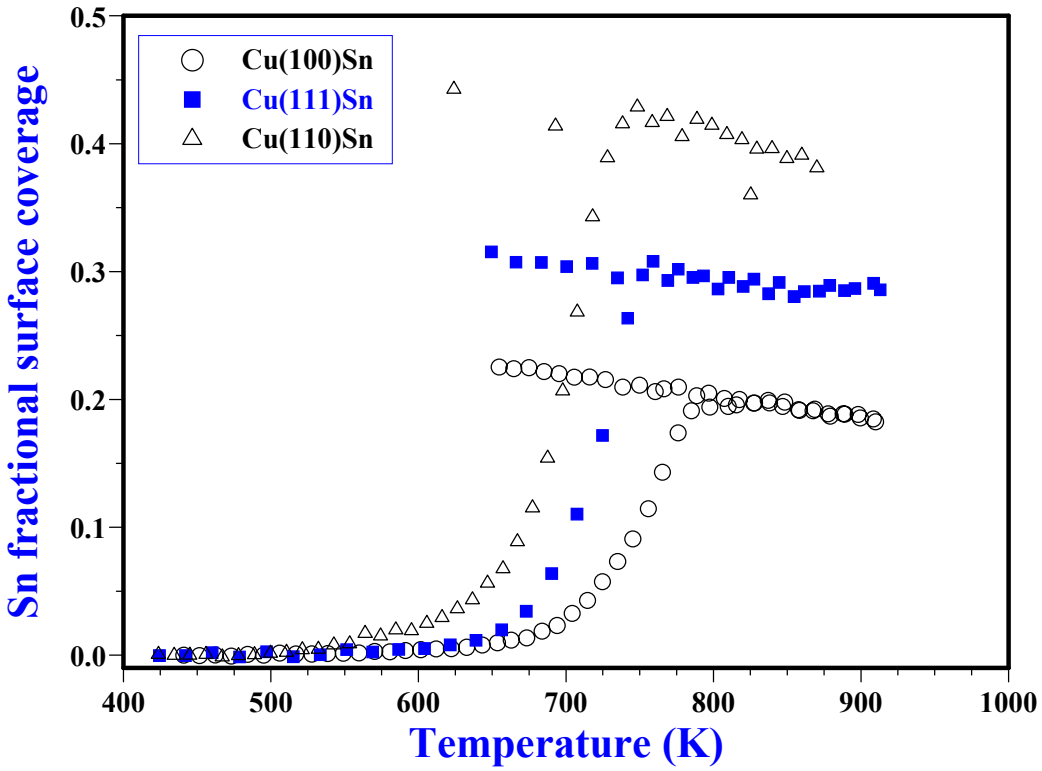

Figure 5.6 Measured Sn segregation profiles in the three different Cu orientations at rates of ± 0.075 K/s

In trying to weigh the effect of the D_o's and E's on the diffusion coefficient D of Sn in the bulk of the three low index planes of Cu, D as a function of temperature T could be written as follows:

Cu(100)Sn,

$$D_{100} = 6.1\times10^{-6}\exp\left(-\frac{189.7}{8.31\times T}\right) \tag{5.1}$$

Cu(110)Sn,

$$D_{110} = 2.8\times10^{-6}\exp\left(-\frac{167.8}{8.31\times T}\right) \tag{5.2}$$

Cu(111)Sn,

$$D_{111} = 9.2\times10^{-4}\exp\left(-\frac{204.6}{8.31\times T}\right) \tag{5.3}$$

For comparison, the plots of D versus T are given in **figure 5.7**.

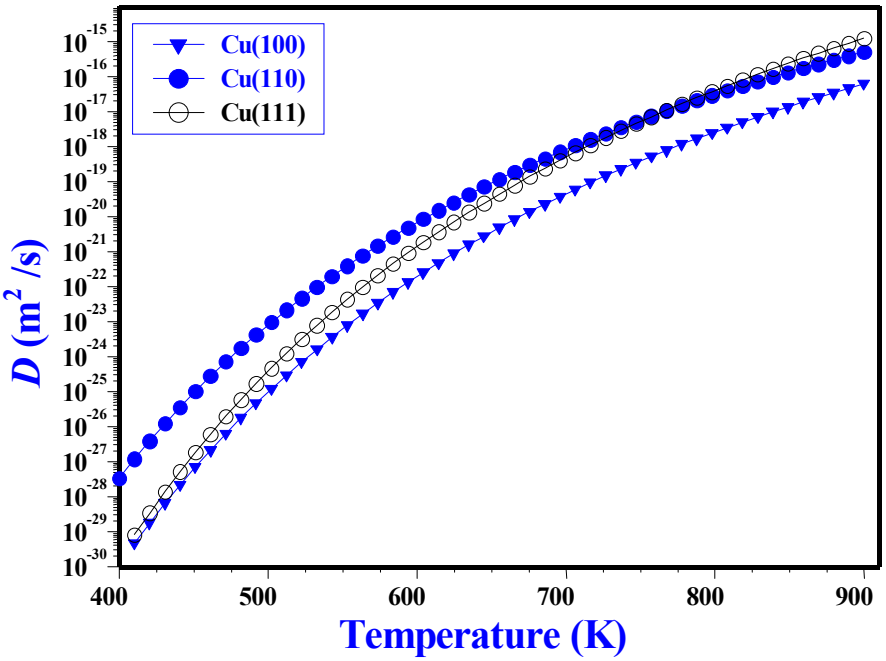

Figure 5.7 The diffusion coefficient of Sn in the three low index planes of Cu as a function of temperature.

Figure 5.7 explicitly portrays the differences in Sn diffusion coefficient in the low index planes of Cu as function of temperature. For all temperatures below 770 K, the bulk diffusion coefficient of Sn is highest in Cu(110). As explained then, both the activation energy and the pre-exponential factor of impurity Sn in Cu(110) are lowest as compared to the other two. Another significant point worth mentioning is the surprising result that Sn bulk diffusion coefficient in Cu(111) is higher than in Cu(100) despite the fact that the activation energy of Sn in Cu(111) is higher than in Cu(100). But from **equations 5.1** and **5.3**, the pre-exponential factor of Sn in Cu(111) is greater than in Cu(100) and that possibly overrides the activation energy factor making the diffusion coefficient of Sn in the former to be higher than that in the latter.

For the first time in segregation measurements, the attractive interaction between Cu and Sn atoms has been determined as 3.8 kJ/mol. See **Table 5.1** for other published segregation parameters besides $\Omega_{\text{Cu-Sn}}$ in the literature.

5.2.4 Comparing published results to the present work

Segregation parameter	D_o (m^2/s)	E (kJ/mol)	ΔG (kJ/mol)	$\Omega_{Cu\text{-}Sn}$ (kJ/mol)	**Technique**	**Reference**
Cu(100)Sn	7.0×10^{-6}	168.0	64 ± 5		Const. temp.	[89]
	1.4×10^{-2}	203.0	63.0		LTR	[83]
	$(6.1 \pm 0.3) \times 10^{-6}$	189 ± 1	65 ± 1	3.9 ± 0.2	LTR	Present study
Cu(110)Sn	5.0×10^{-5}	178.0	72 ± 5		Const. temp.	[89]
	3.0×10^{-3}	205.0	72.0		LTR	[83]
	$(2.8 \pm 0.3) \times 10^{-6}$	167.8	62.3 ± 1	3.8 ± 0.2	LTR	Present study
Cu(111)Sn	2.0×10^{-6}	176.0	67.0		Const. temp.	[45]
	9.0×10^{-5}	172.0	76 ± 5		Const. temp.	[89]
	1.5×10^{-1}	234.0	78.0		LTR	[83]
	$(9.2 \pm 0.3) \times 10^{-4}$	204.6	69.5 ± 1	3.8 ± 0.2	LTR	Present study

Table 5.1 Published results compared to the present study

As was mentioned in **Chapter One**, the present study is unique on two counts. Firstly, all the three samples were fabricated to have the same Sn bulk concentration. The second point is that all the segregation measurements were taken under the same experimental conditions. It is clear from **Table 5.1** that the segregation parameters of Sn obtained for the present study compare fairly well with other published results.

5.3 The ternary CuSnSb system

Having seen the segregation behaviour of Sn in the three low index planes of Cu, the question arises what would happen if another low concentration alloying element was introduced to the binary Cu-Sn alloy systems to form ternary systems. Sb was the element added to Cu(100)-Sn and Cu(111)-Sn binary alloys to convert them into ternary alloy systems. As expected there was a change in the segregation behaviour of Sn brought about by the addition of Sb in both ternary alloys. There were also differences in the combined segregation profiles of Sn and Sb in the two Cu crystals.

Like Sn, Sb has a larger atomic size than Cu. Sb is a pentavalent atom and as discussed before (**section 5.2**), that is, from the point of view of size mismatch and electronic factors, it can segregate to the surface of a thermally activated CuSb binary alloy system [88-91].

Earlier studies on Cu(111)-0.133 at% Sn-0.180 at. % Sb ternary alloy system [92] have shed some light on the segregation behaviours of Sn and Sb. Sn is known to have a higher diffusion coefficient than Sb and as a result will segregate first to the surface of Cu(111) in a phenomenon called sequential segregation.

Typical Sn and Sb segregation profiles in Cu are given in **figure 5.8**.

5.3.1 Sn and Sb segregation profiles in Cu single crystal

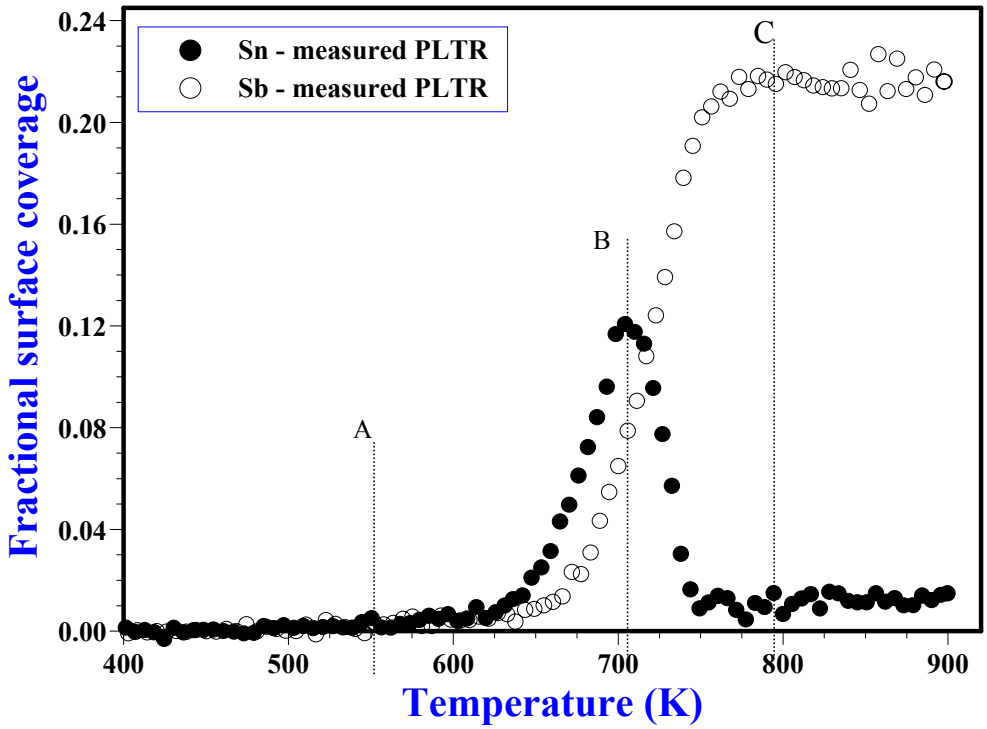

Figure 5.8 A typical measured PLTR run of Sn and Sb segregation profile in Cu(100) at 0.075 K/s rate showing four regions.

Similar to **figure 5.1**, four main regions could be identified from the Sn and Sb segregation profiles in **figure 5.8**. The region below the temperature line A has low temperatures and therefore the diffusion coefficients D_{Sn} and D_{Sb} are small and as a result the AES system does not detect any appreciable amount of Sn and Sb on the surface of the Cu crystal at these small time intervals (0.075 K/s). In the region between A and B, however, the D values of the segregating species increase exponentially and the fluxes of Sn and Sb atoms increase from the bulk to the surface. Sn starts with a higher surface concentration and build-up untill it reaches a maximum concentration at the temperature

line B. The possible reason lies in the fact that E_{Sn} = 175.2 kJ/mol is less than E_{Sb} = 186.3 kJ/mol

The interaction energy between the atoms of the three elements; $\Omega_{Cu\text{-}Sn}$ = 3.4 kJ/mol, $\Omega_{Cu\text{-}Sb}$ = 16.1 kJ/mol and $\Omega_{Sn\text{-}Sb}$ = -5.3 kJ/mol, coupled with the segregation energies have a profound effect on the segregation profiles of Sn and Sb, particularly toward and inside the equilibrium region, from higher temperatures above line B. The repulsive interaction between the segregating Sn and Sb ($\Omega_{Sn\text{-}Sb}$ = -5.3 kJ/mol) causes the latter to desegregate as the temperature increases further at B. Sb with a higher segregation energy, ΔG_{Sb} = 84.3 kJ/mol as against ΔG_{Sn} = 64.5 kJ/mol will sequentially displace Sn from the surface in the region between lines B and C. Site competition of Sn and Sb atoms could be another avid description in this temperature region and beyond. The differences in the chemical potential energies between the surface and bulk layers that are due to the combined effect of the energetic factors, namely, the segregation and the atomic interaction energies and the surface concentrations, of both Sn and Sb are rapidly approaching zero as the temperature increases and approach the temperature line C. Thus, the kinetic segregation region could be defined as the profiles occupying the temperature region between the temperature lines A and C. Beyond the temperature line C, the differences in the changes in the chemical potential energy between the surface layer and the first bulk layer and between the rests of the bulk layers become zero. The values of the surface concentrations of both Sn and Sb remain the same, implying that their net fluxes are zero. An equilibrium segregation region could then be defined as the higher temperature region from the temperature line C for the PLTR segregation profile. **Figure 5.9** shows these equilibrium segregation profiles for the PLTR and NLTR runs.

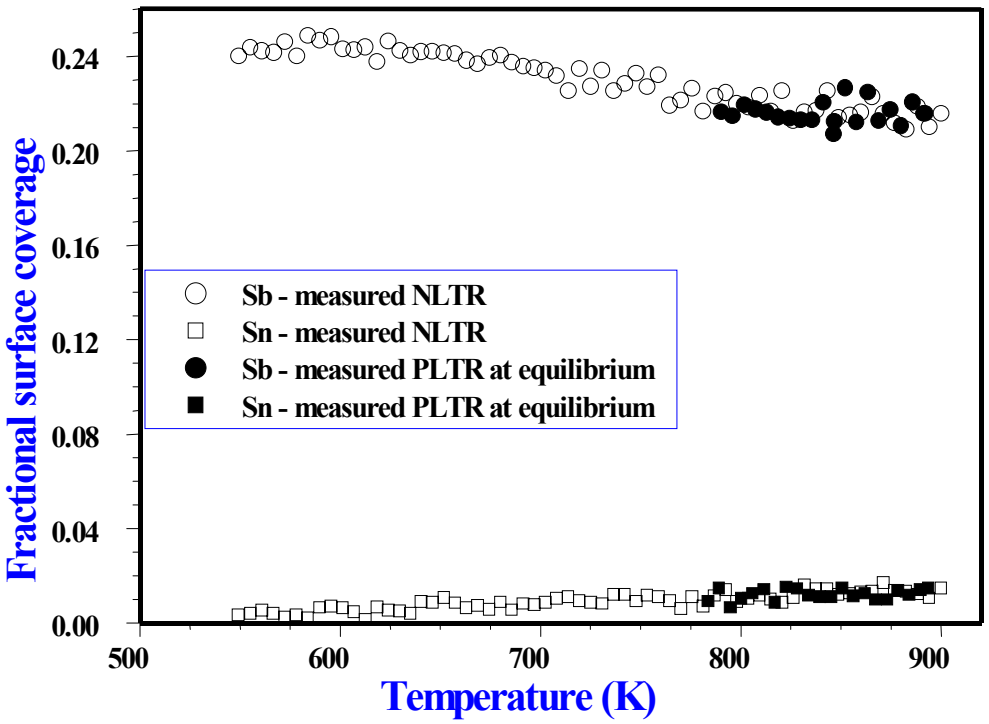

Figure 5.9 A typical measured NLTR run (open symbols) of Sn and Sb segregation profiles in Cu(100) at -0.075 K/s rate. The narrow regions of the PLTR run (closed symbols) are also shown.

The proof of the NLTR runs as the equilibrium profile was ascertained with another PLTR run immediately after the end of the NLTR run. The data points of the second PLTR run profiles are within experimental error the same as the NLTR.

The set of fit values generated when the Guttman segregation equations were used to fit the narrow-equilibrium-temperature part of the PLTR profile were not unique because of the slowly changing, "stiff", profile and narrow temperature range involved. However, by extending the equilibrium region over a larger temperature range, by using a NLTR run, a much better set of segregation and interaction energies could be found mathematically as was shown in **figure 4.14** of **section 4.3.1**.

The effect of different heating and cooling rates on the segregation of Sn and Sb are given in **figures 5.10** and **5.11** for Cu(100) and Cu(111) crystals respectively. Like the segregation profiles of Sn in the binary CuSn alloy, (see **figures 5.2**, **5.3**, and **5.4**), the PLTR segregation profiles of Sn and Sb in the ternary alloys shift to higher temperatures as the heating rate of the crystal increases.

5.3.2 Sn and Sb segregation profiles at different rates

5.3.2.1 Cu(100)

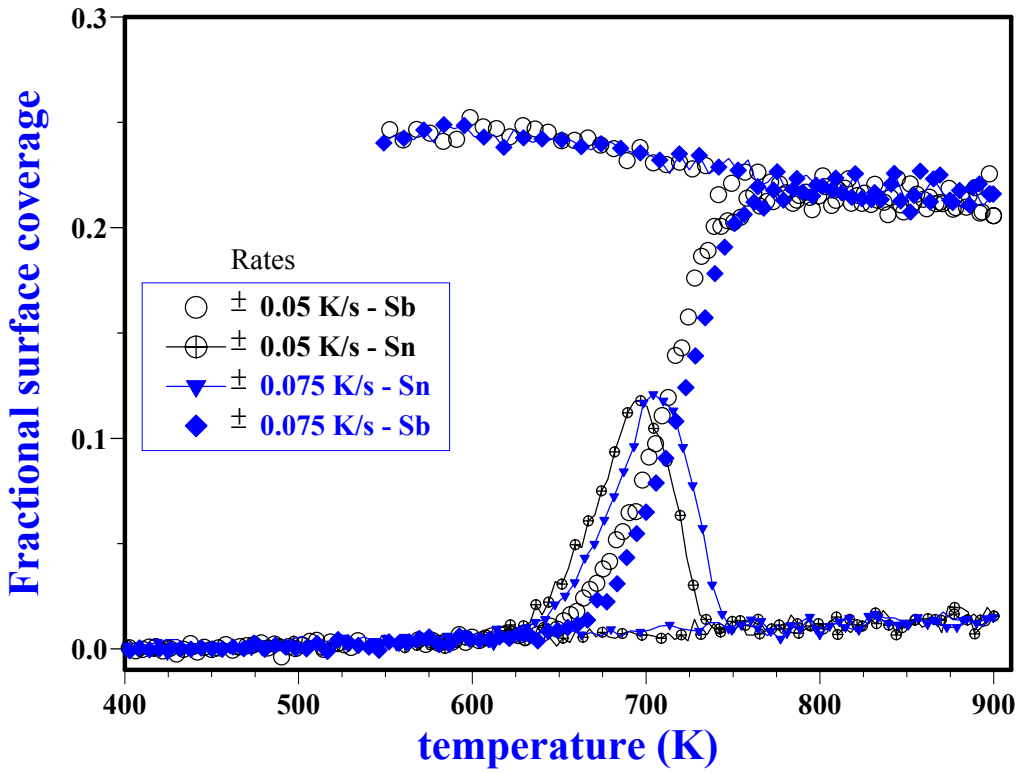

Figure 5.10 Measured Sn and Sb segregation profiles in Cu(100) at different heating (PLTR) and cooling (NLTR) rates.

5.3.2.2 Cu(111)

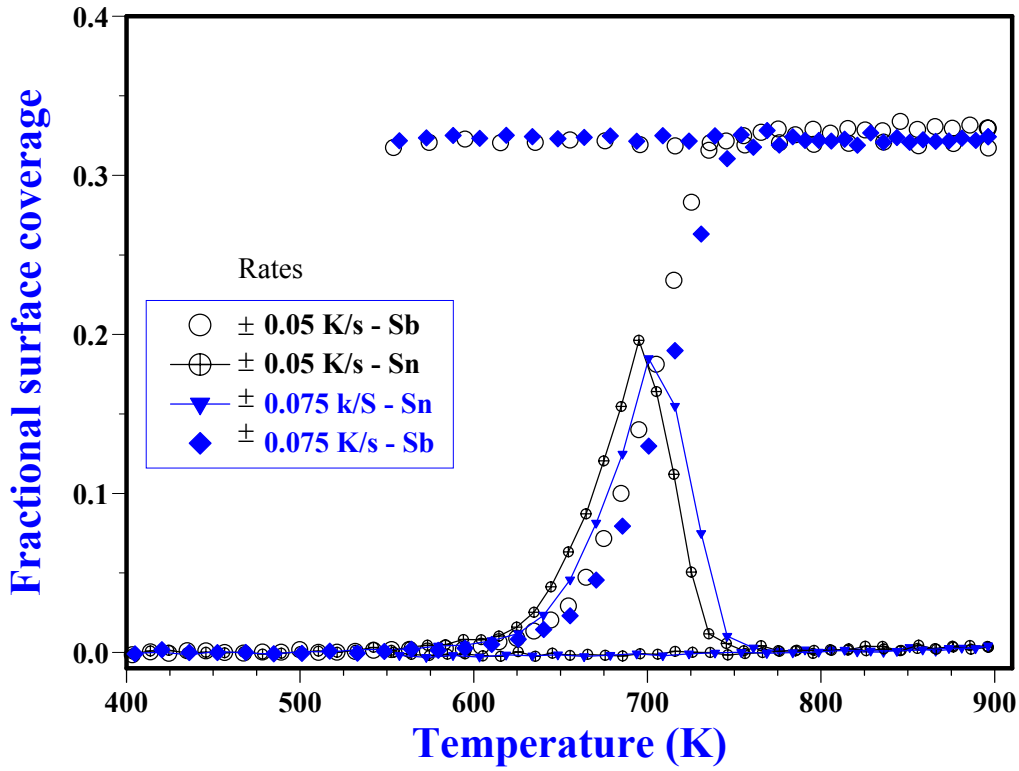

Figure 5.11 Measured Sn and Sb segregation profiles in Cu(111) at different heating and cooling rates.

It should be noted that the cooling, NLTR profiles, are independent of the "low" cooling rates used. Measurements were also taken from PLTR and NLTR runs at rates of ± 0.15 K/s respectively and the PLTR profile lies to the right of 0.075 K/s PLTR profile at higher temperatures. Similar observations were found for Sn segregation in binary Cu(100)Sn alloy [93].

Having considered the segregation profiles of Sn and Sb in the two orientations namely, Cu(100) and Cu(111) crystals separately, they can further be compared at a chosen rate. This is done in the next **section 5.3.3**.

5.3.3 Sn and Sb segregation profiles in Cu(100) and Cu(111) at the same rate

5.3.3.1 Crystals heating rate at 0.05 K/s

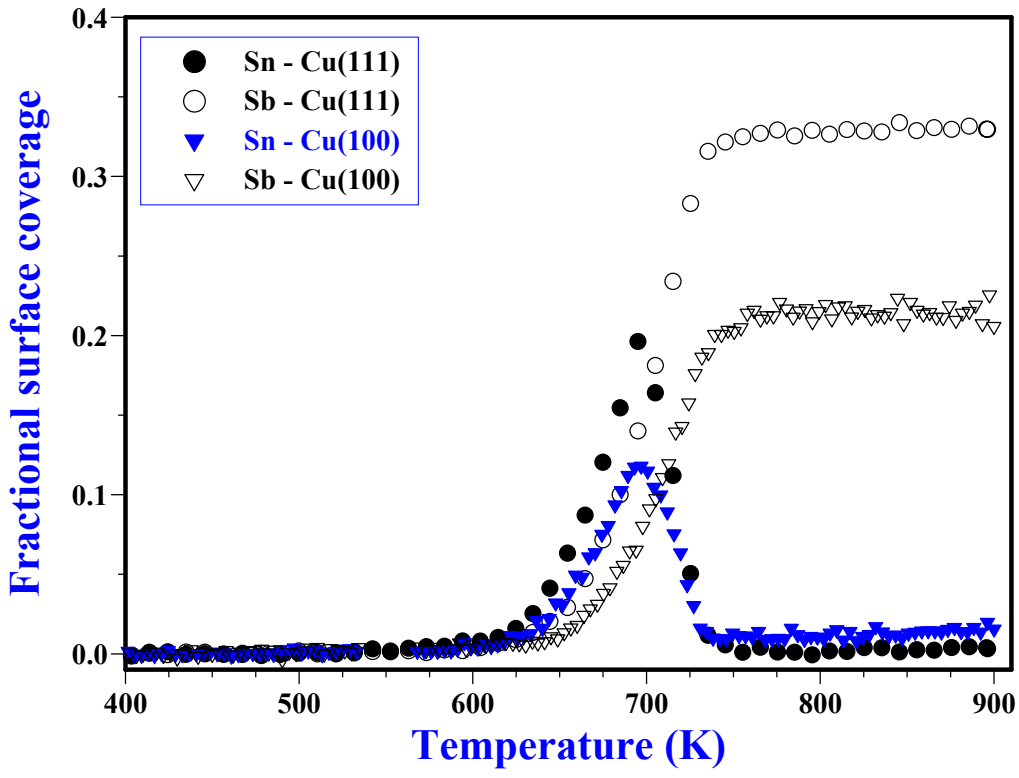

Figure 5.12 Measured Sn and Sb segregation profiles in Cu(100) and Cu(111) at the same heating rate of 0.05 K/s. Notice the Sn and Sb pair in Cu(111) lying at lower temperatures.

The segregates first appear on the surface of Cu(111) at relatively lower temperatures as compared to their appearance on Cu(100). Interestingly, a similar trend was seen when the binary Cu(100)Sn and Cu(111)Sn alloys were compared (see **figures 5.5** and **5.6**). It is to be expected then that the set of diffusion parameters of Sn and Sb in the two Cu orientations will differ. Taking the segregation parameters of Sb as found for both Cu(100) as well as Cu(111) into consideration, the pre-exponential factors, $D_{oSb(Cu(100)} = 2.8 \times 10^{-5}$ m^2s^{-1} is two orders of magnitude lower than $D_{oSbCu(111)} = 3.4 \times 10^{-3}$ m^2s^{-1}. This justifies the Sb segregation profile in Cu(111) lying at lower temperatures to that in Cu(100) notwithstanding the fact that $E_{SbCu(100)} = 186$ kJ/mol is lower than $E_{Sb}(111) = 206$ kJ/mol. It simply means that the diffusion coefficient of Sb in Cu(111) is higher than in Cu(100) on the strength of higher D_o. Similar explanations also hold for Sn in the two Cu orientations. The other result for the heating rate of 0.075 K/s is shown in **figure 5.13**.

5.3.3.2 Crystals heating rate at 0.075 K/s

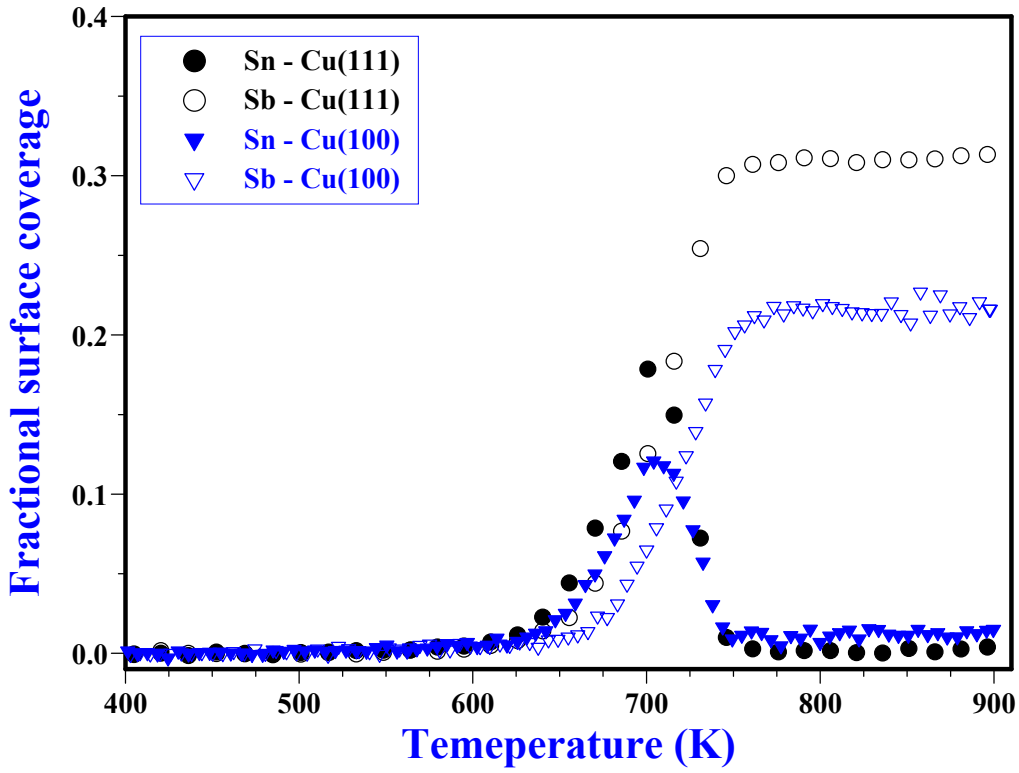

Figure 5.13 Measured Sn and Sb segregation profiles in Cu(100) and Cu(111) at the same heating rate of 0.075 K/s.

Figures 5.12 and **5.13** clearly show that Sn and Sb segregating set in Cu(111) lie at lower temperatures (to the left of the Cu(100) profiles).

The next step is to follow the trend of Sn segregation in Cu(111) (binary alloy) and in Cu(111)Sb (ternary alloy). **Figure 5.14** shows the profiles of the two systems.

5.3.4 Comparing Sn in binary CuSn to Sn in ternary CuSnSb

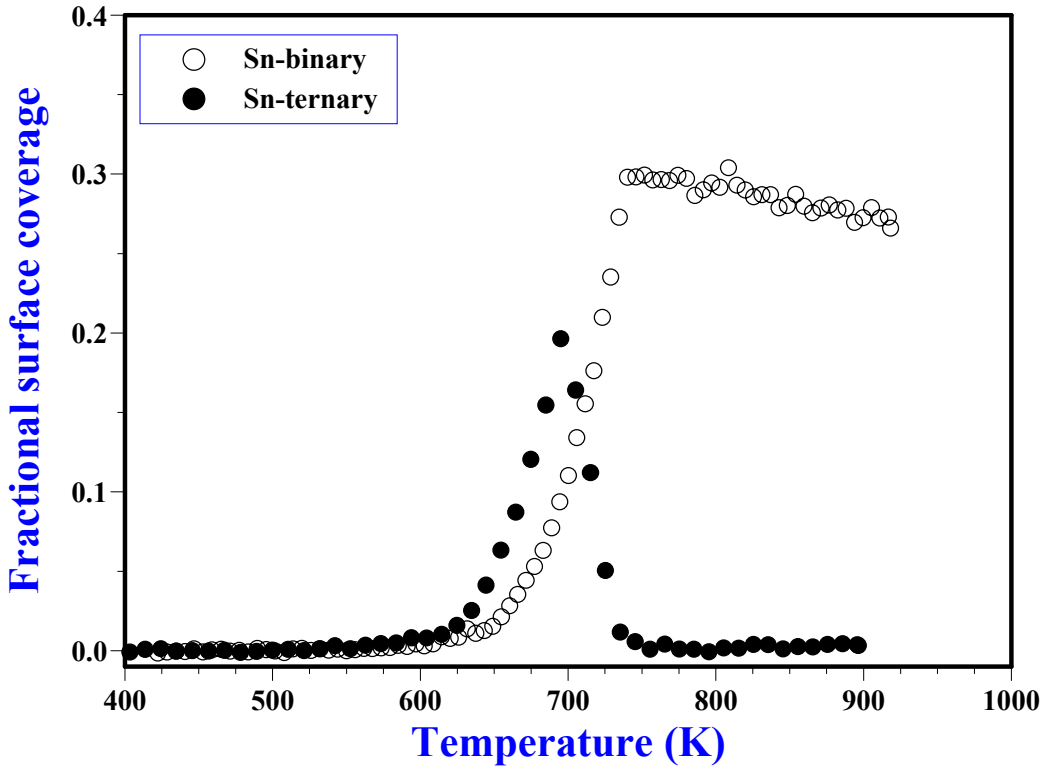

Figure 5.14. Measured Sn segregation profiles in the binary (open circle) Cu(111)Sn and ternary (closed circle) Cu(111)SnSb. The heating rate was 0.075 K/s.

It is seen that the segregation profile of Sn in the ternary alloy lie at lower temperatures as compared to the profile in the binary. Perhaps the first possible explanation lies in the differences in the interaction energies between the three atoms. As explained earlier, both Sn and Sb segregate strongly in Cu and have attractive interactions with Cu atoms ($\Omega_{Cu\text{-}Sn}$ = 3.4 kJ/mol, $\Omega_{Cu\text{-}Sb}$ = 16.1 kJ/mol) but repulsive interaction between themselves ($\Omega_{Sn\text{-}Sb}$ = -5.3 kJ/mol). Sn segregating first in the ternary could be attributed to its

weaker attractive interaction with Cu and is further aided by the repulsive interaction between the atoms of Sn and Sb. Sn in the ternary alloy is seen desegregating as a result of the stronger segregation energy of Sb and the repulsive interaction between the segregating elements. The second explanation would lie in a change in the activation energy of Sn in the binary and in the ternary systems. The addition of Sb solute that is also bigger in size than the matrix Cu atoms would elastically strain and expand the Cu lattice further. Vacancies would then be attracted to the Sb and the Sn atoms and result in the decrease in the vacancy formation energy [94]. Also, the expansion of the lattice would imply that the energy required by an atom to "squeeze" through the saddle point would be reduced. In these circumstances, the activation energy of the Sn solute that is made up of the migration and the vacancy formation energies would decrease and increase the diffusion rate of Sn in the ternary alloy. The results in **Table 4.2** show $E_{Sn(binary)}$ = 205 kJ/mol as against $E_{Sn(ternary)}$ = 196 kJ/mol and explains the kinetic segregation region of the two profiles.

5.4 What has evolved in the course of this study

1. In July 2001, at South African Institute of Physics (SAIP) annual conference at the University of Natal, Durban, a poster presentation was given entitled:

   "A Mathematical fit procedure to determine segregation parameters from experimental data of a linear temperature run".

   Authors: Asante JKO; Terblans JJ; Roos WD.

2. In September 2002, a poster entitled, "A reliable method for finding the equilibrium segregation parameters in a ternary system" was presented at SAIP annual conference at Potchefstroom University.

Authors: JKO Asante; WD Roos; JJ Terblans.

3. An oral presentation entitled, "Segregation parameters in a (111)CuSnSb crystal from constant temperature runs" was given at SAIP annual conference at University of Stellenbosch in June 2003.

Authors: JKO Asante; WD Roos; JJ Terblans.

4. Attended and presented a paper entitled "Finding the equilibrium segregation parameters in a Cu(111)SnSb ternary system" at the **Fourth International Workshop on Surface & Interface Segregation** in August 2003, at iThemba LABS, in Cape Town.

   Authors: JKO Asante; WD Roos; JJ Terblans.

5. In June, 2004, an oral presentation was given at the annual SAIP conference title, "An AES study of Sn surface segregation in the low index planes of Cu single crystals" at the University of the Free State, Bloemfontein.

   Authors: JKO Asante; WD Roos; JJ Terblans.

6. A paper entitled, "An AES study of Sn surface segregation in Cu single crystals" has been published in the *Surface and Interface Analysis* 2005; **37**:517-521.

   Authors: JKO Asante, JJ Terblans and WD Roos.

7. Another paper entitled, “Segregation of Sn and Sb in a ternary Cu(100)SnSb alloy” has been accepted for publication in *Applied Surface Science* on 4 March 2005. Authors: JKO Asante, JJ Terblans and WD Roos.

8. A paper entitled, “Segregation of Sn in the binary Cu(111)Sn and ternary Cu(111)SnSb alloy systems” is in preparation.

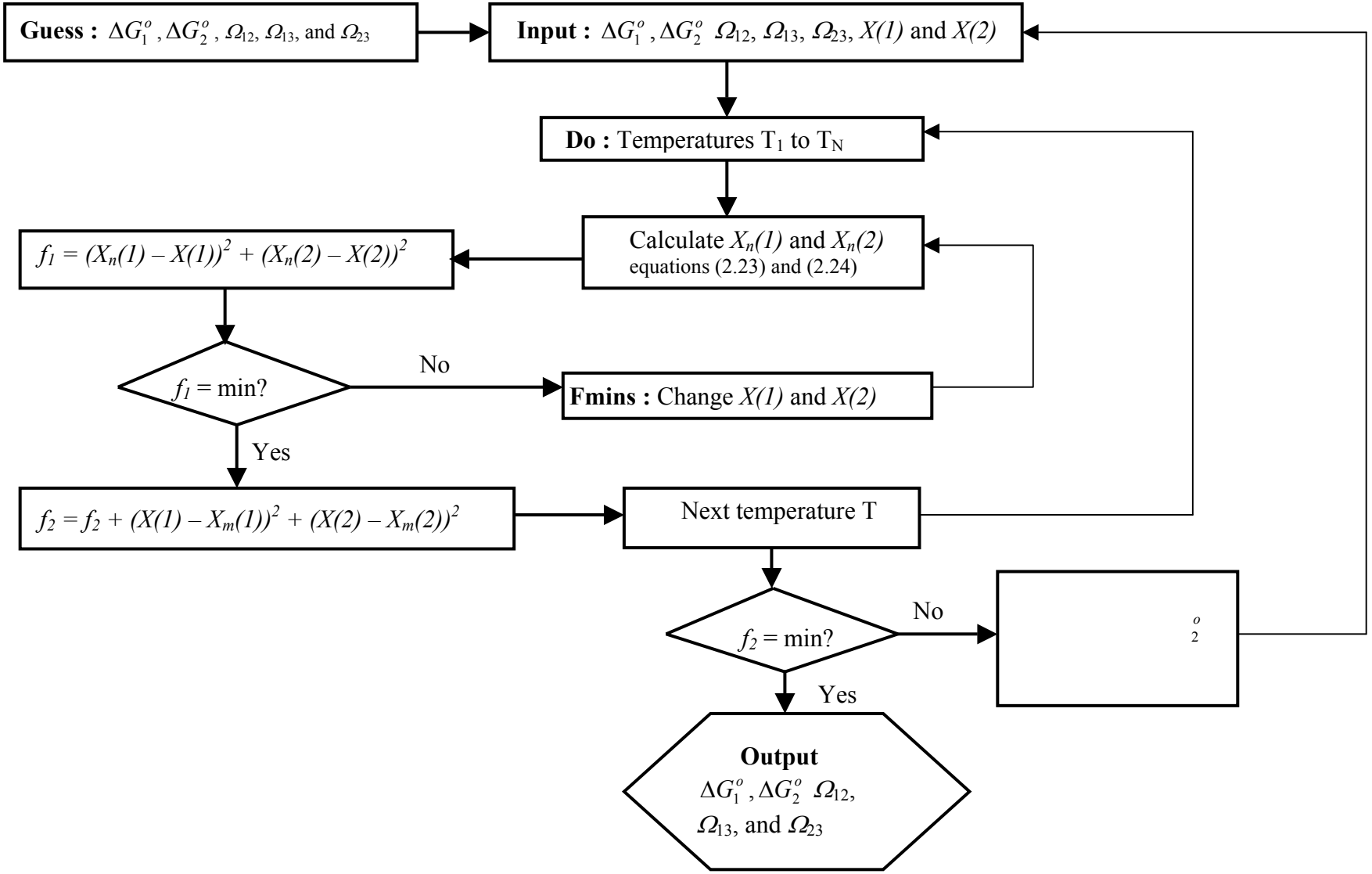

Appendix A: The solution to Guttman equilibrium segregation equations

BIBLIOGRAPHY

1. D. Kalderon, Proc. Instn. Mech. Engrs. **186**, 1972, 341.
2. M.P. Seah, Surf. Sci. **80**, 1979, 8.
3. D. Briggs and M.P. Seah eds, *Practical Surface Analysis, 2nd ed.* **1**, John Willey and Sons, 1990, 313.
4. M.P. Seah, J. Phys. F: Metal Phys. **10**, 1980, 1059.
5. P.E. Irving, M.P.Seah and A. Kurzfeld, *Proc. 2nd Int. Conf. On Mechanical Behaviour of Materials,* 1976, Boston: ASM, 563-7.
6. C.J. Simpson, W.C. Winegard and K.T. Aust, *Grain boundary Structure and Properties*, ed. G.A.Chadwick and D.A. Smith, (London: Aca. Press), 1976, 201-34.
7. H. Gleiter and **B.** Chalmers, Prog. Mater. Sci. **16**, 1972, 77-112.
8. M.P. Seah, J.Catal. **57**, 1979, 450-7.
9. A. Joshi and D.F. Stein, Corros. **28**, 1972, 321-30.
10. C. Lea, M.P. Seah and E.D. Hondros, Mater. Sci. Eng. **42**, 1980, 233-44.
11. K. Yoshino and C.J. McMahon, Metall. Trans. **5**, 1974, 363-70.
12. http://www.connector.org/timecompounds03.html.
13. http://www.connector.org/coppertin03.html.
14. M.A. Nicolet, Thin Sol. Films, **52**, 1978, 415-43.
15. F.M. d'Heurle, A. Gangulee, *The nature and Behaviour of Grain Boundaries*, Ed. H. Hu, (New York: Plenum), 1972, 339-65.
16. A.Rodnyansky, Y.J. Warburton and L.D. Hanke, Surf. Inter. Anal. **29**, 2000, 215.
17. C Uebing, H. Viefhaus and H.J Grabke: *Surface Segregation and Related Phenomena,* Eds. P. Dowben and A. Miller, CRC Press, Boca Raton, Fl, 1990, 241.
18. H. Viefhaus, J. Peters and H.J. Grabke, Surf. Inter. Anal. **10**, 1987, 280.
19. C. Uebing, Surf. Sci. **225***,* 1990, 97.
20. C. Uebing, H. Viefhaus and H.J. Grabke, Surf. Sci. **264**, 1992, 114.
21. C. Uebing and H. Viefhaus, Surf. Sci. **236**, 1990, 29.

22. Ch. Muller, Ch. Uebing, M. Kottcke, Ch. Rath, L. Hammer and K. Heinz, Surf. Sci. **400**, 1998, 87.
23. R.D. Choudhuri and A. Miller: *Surface Segregation and Related Phenomena,* Eds. P. Dowben and A. Miller, (Boca Raton, Fl.: CRC Press) , 1991.
24. G. Wang, M.A. Van Hove, P.N. Ross and M.I. Baskes, http://repositories.cdlib.org./lbnl/LBNL-54839, 2004.
25. J. Arenas-Alatorre, M. Avolos-Borja and G. Diaz, Appl. Surf. Sci. **189**, 2002, 7.
26. J.W. Gibbs, *The Scientific papers of J.W. Gibbs* **1** (New York: Dover), 1961, 219.
27. S. Hofman, Scan. Electron. Microsc., **3**, 1985, 1071.
28. A.V. Ruben and H.L.Skriver, Comp. Mat. Sci. **15**, 1999, 127.
29. G. Bozzolo, J. Ferrante, R.D. Noebe, B. Good, F.S. Honecy, P. Abel, Comp. Mat. Sci. **15**, 1999, 177.
30. J. Nyéki, Ch. Girardeaux, Z. Erdélyi, G.A. Langer, G. Erdélyi, D.L. Beke and A. Rolland, Surf. Sci. **495**, 2001, 200.
31. P.G. Shewmon, *Diffusion In Solids*, McGraw-Hill, New York, 1963, 61.
32. J.J. Terblans, Surf. Inter. Anal. **33**, 2002, 767.
33. E.C Viljoen and J. du Plessis, Surf. Sci. **431**, 1999, 128.
34. N.-H. Heo, Acta. Mat. **44**, 1996, 1581.
35. J. du Plessis, *Surface Segregation,* Diffusion and Defect Data Vol. 11, Sci-Tech Pub. Ltd., **9**, 1990, 125.
36. L.S. Darken Trans. AIME, **180**, 1949, 430.
37. G.N. van Wyk, J. du Plessis and E. Taglauer, Surf. Sci., **255**, 1991, 73.
38. J. du Plessis, Appl. Surf. Sci., 70/71, **303**, 1993, 307.
39. S. Hofman and J. Erlewein, Surf. Sci., **77**, 1978, 591.
40. A.D Brailsford, Surf. Sci., **94**, 1980, 387.
41. J. du Plessis and G.N. Van Wyk, J. Phys. Chem. Solids, **50**, 1989, 237.
42. M. Menyhard, Surf. Interf. Anal. **19**, 1992, 615.
43. M. M. Eisl, B.M. Reichl and H. Stori, Applied Surf. Sci., **70/71**, 1993, 137.
44. S. Hofmann and J. Erlewein, Scripta. Met., **10**, 1976, 857.
45. S. Hofmann and J. Erlewein, Surf. Sci. **77**, 1978, 591.
46. F. J. Mojica and L. L. Levenson, Surf. Sci. **59**, 1976, 447.
47. G.L.P. Berning and W.J. Coleman, Surf. Sci. **173**, 1986, 411.
48. W.E. Delport and J.P. Roux, Corros. Sci. **26**, 1986, 407.
49. J. du Plessis and P.E. Viljoen, Surf. Sci. **131**, 1983, 321.

50. E.C. Viljoen, and J.du Plessis, Surf. Interf. Anal. **22**, 1994, 598.
51. J. du Plessis and E.C. Viljoen, Appl. Surf. Sci. **59,** 1992, 171.
52. M.M. Eisl, B.M. Reichl and H. Stori, Surf. Sci., **336**, 1995, 379.
53. J.H. Hildebrand and R.L. Scott *The Solubility of Nonelectrolytes,* 3rd. ed., Van Nostrand Reinhold, New York, 1950.
54. J. du Plessis and G. N. Van Wyk, J. Phys. Chem. Solids, **49,** 1988, 1442.
55. M. Gutmann, Surf. Sci. **53**,1975, 213.
56. J.K.O. Asante, J.J. Terblans and W.D. Roos, article submitted for publication 2004.
57. L.S. Darken, Trans. AIME **180,** 1949, 430.
58. J. du Plessis, *Surface Segregation,* Diffusion and Defect Data Vol.11, Sci-Tech Pub. Ltd., **9**,1990, 70.
59. H. Viefhuas and M. Rüsenberg, Surf. Sci. **159**, 1985, 1.
60. M.J. Spaarnay, Surf. Sci. Rep. **4**, 1985, 101.
61. M. Gutmann, Surf. Sci. **53**,1975, 216.
62. Material-Technologie & Kristalle, Büro für Forshungsmaterialien, Karl-Heinz-Beckurts-Strasse 13, D52428, Jülich, Germany.
63. Goodfellow Cambridge Limited, Cambridge CB4, 4DJ, England.
64. J. Crank, *The Mathematics of Diffusion,* 2nd edition, Clarendon, Oxford, 1975.
65. J. du Plessis and P.E. Viljoen, Surf. Sci. Let. **276**, 1993, L9.
66. W. Arabczyk, M. Militzer, H.J. Müssig and J. Wieting, Surf. Sci. **198**, 1988, 169.
67. J. Nyéki, Ch. Girardeaux, Z. Erdélyi, G.A. Langer, G. Erdélyi, D.L. Beke and A. Rolland, Surf. Sci. **495**, 2001, 200.
68. L.S. Chang, E. Rabkin, S. Hofmann and W. Gust, Acta. Mater. **10**, 1999, 2951.
69. M.M. Eisl, B. M. Reichl, H. Stori, Surf. Sci. **336,** 1995, 379.
70. J.K.O. Asante, J.J. Terblans and W.D. Roos, Surf. Inter. Anal. **37**, 2005, 517.
71 D. Briggs and M.P. Seah (eds.) *Practical Surface Analysis,2nd ed.* **1**,Wiley, New York, 1990, 208.
72. H. Viefhaus and M. Rüsenberg, Surf. Sci. **159**, 1985, 1.
73. E.C. Viljoen, J.du Plessis, H. C. Swart and G. N. van Wyk, Surf. Sci. **342**, 1995, 3.
74. H. Giordano, J.P. Bibérian, B. Aufray, Surf. Sci. **313**, 1994, 269.
75. J.K.O. Asante, J.J. Terblans and W.D. Roos, *Accepted for publication in* Appl. Surf Sci. 2005.
76. J.J. Terblans, Surf. Inter. Anal. **33**, 2002, 769.

77. MATLAB, *The Language of Technical Computing*, Version 5. The Math Works Inc., Natick, MA, 1999.
78. J. Borg and G.T. Diens, *An Introduction to Solid State Diffusion,* Academic Press, San Diego, 1988, 45.
79. P.G. Shewmon, *Diffusion In Solids,* McGraw-Hill, New York, 1963, 44.
80. M.M. Eisl, B. M. Reichl, H. Stori, *Surf. Sci.* **336,** 1995, 379.
81. J.K.O. Asante, J.J. Terblans and W.D. Roos, Surf. Inter. Anal. **37**, 2005, 520.
82. E.C. Viljoen and J. du Plessis, Surf. Sci., **468**, 2000, 33.
83. J.J. Terblans, Surf. Inter. Anal. **33**, 2002, 767.
84. N.I. Papanicolaou and D.A. Papaconstantopoulos, Th. Solid Films, **428**, 2003, 42.
85. J. J. Terblans, PhD Thesis, UFS, Bloemfontein, 2002.
86. R.J. Borg and G.T. Diens, *An Introduction to Solid State Diffusion,* Academic Press, San Diego, 1988, 63.
87. C.P. Flynn, *Point Defects and Diffusion,* Clarendon Press, Oxford, 1972.
88. J. du Plessis, Appl. Surf. Sci., **100/101**, 1996, 222.
89. W.J. Erasmus, MSc Thesis, UFS, Bloemfontein, 1999.
90. H. Giordano, J.P. Bibérian, B. Aufray, Surf. Sci. **313**, 1994, 266.
91. J.K.O. Asante, W.D. Roos and M.F. Maritz, Surf. Interf. Anal., **31**, 2001, 856.
92. J.K.O. Asante, W.D. Roos and J.J. Terblans, Surf. Interf. Anal., **35**, 2003, 441.
93. J. du Plessis and E.C. Viljoen, Appl. Surf. Sci. **59,** 1992, 173.
94. P.G. Shewmon, *Diffusion In Solids,* McGraw-Hill, New York, 1963, 96.